Cell Stem Cell

Article

Antigen presentation safeguards the integrity of the hematopoietic stem cell pool

Graphical abstract

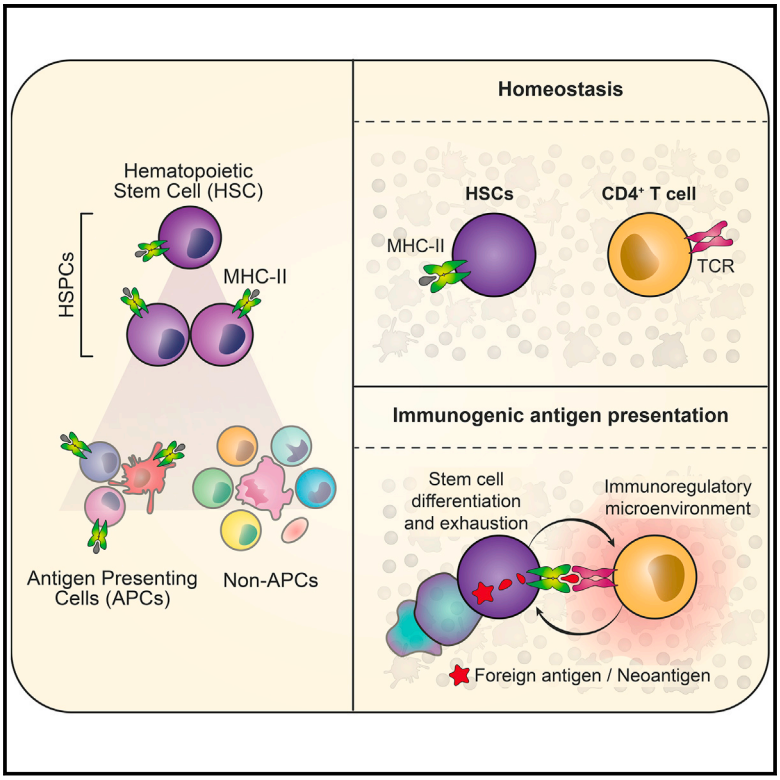

Highlights

- HSPCs constitutively present antigens via MHC-II
- Presentation of immunogenic antigens results in the activation of CD4$^+$ T cells
- Antigen presentation causes differentiation and depletion of immunogenic HSPCs
- This prohibits the onset of HSC-derived leukemias presenting neoantigens via MHC-II

Authors

Pablo Hernández-Malmierca, Dominik Vonficht, Alexandra Schnell, ..., Andreas Trumpp, Vijay K. Kuchroo, Simon Haas

Correspondence

a.trumpp@dkfz.de (A.T.), vkuchroo@evergrande.hms.harvard.edu (V.K.K.), simon.haas@bih-charite.de (S.H.)

In brief

Haas and colleagues show that hematopoietic stem cells (HSCs) act as antigen-presenting cells. The presentation of immunogenic antigens triggers a bidirectional interaction with antigen-specific CD4$^+$ T cells, resulting in the rapid exhaustion of diseased HSCs, thereby safeguarding the integrity of the stem cell pool.

Hernández-Malmierca et al., 2022, Cell Stem Cell *29*, 760–775
May 5, 2022 © 2022 Elsevier Inc.
https://doi.org/10.1016/j.stem.2022.04.007

CellPress

CellPress

Cell Stem Cell

Article

Antigen presentation safeguards the integrity of the hematopoietic stem cell pool

Pablo Hernández-Malmierca,[1,2,3,23] Dominik Vonficht,[1,2,3,23] Alexandra Schnell,[4,5,23] Hannah J. Uckelmann,[6,7] Alina Bollhagen,[1,2] Mohamed A.A. Mahmoud,[1,2] Sophie-Luise Landua,[1,2] Elise van der Salm,[1,2] Christine L. Trautmann,[1,2] Simon Raffel,[8] Florian Grünschläger,[1,2,3] Raphael Lutz,[1,2,8] Michael Ghosh,[9] Simon Renders,[1,2,8] Nádia Correia,[1,2] Elisa Donato,[1,2] Karin O. Dixon,[4,5] Christoph Hirche,[1,10] Carolin Andresen,[1,2,3] Claudia Robens,[1,2] Paula S. Werner,[1,10] Tobias Boch,[1,2,11,12] David Eisel,[13] Wolfram Osen,[13] Franziska Pilz,[1,10] Adriana Przybylla,[1,2] Corinna Klein,[1,2] Frank Buchholz,[14] Michael D. Milsom,[1,15] Marieke A.G. Essers,[1,10] Stefan B. Eichmüller,[13] Wolf-Karsten Hofmann,[11,12] Daniel Nowak,[11,12] Daniel Hübschmann,[1,16,17] Michael Hundemer,[8] Christian Thiede,[17,18] Lars Bullinger,[17,19] Carsten Müller-Tidow,[8,20] Scott A. Armstrong,[6,7] Andreas Trumpp,[1,2,17,*] Vijay K. Kuchroo,[4,5,*] and Simon Haas[1,2,17,19,21,22,24,*]

[1]Heidelberg Institute for Stem Cell Technology and Experimental Medicine (HI-STEM gGmbH), Heidelberg, Germany
[2]Division of Stem Cells and Cancer, Deutsches Krebsforschungszentrum (DKFZ), and DKFZ-ZMBH Alliance, Heidelberg, Germany
[3]Faculty of Biosciences, Heidelberg University, Heidelberg, Germany
[4]Evergrande Center for Immunologic Diseases, Harvard Medical School, and Brigham and Women's Hospital, Boston, MA, USA
[5]Klarman Cell Observatory, Broad Institute of MIT and Harvard, Cambridge, MA, USA
[6]Department of Pediatric Oncology, Dana-Farber Cancer Institute, and Division of Hematology/Oncology, Boston, MA, USA
[7]Boston Children's Hospital and Harvard Medical School, Boston, MA, USA
[8]Department of Hematology, Oncology and Rheumatology, University of Heidelberg, Heidelberg, Germany
[9]Department of Immunology, Institute for Cell Biology, University of Tübingen, Tübingen, Germany
[10]Division of Inflammatory Stress in Stem Cells, Deutsches Krebsforschungszentrum (DKFZ) and DKFZ-ZMBH Alliance, Heidelberg, Germany
[11]Department of Hematology and Oncology, University Hospital Mannheim, Mannheim, Germany
[12]Medical Faculty Mannheim, Heidelberg University, Mannheim, Germany
[13]Research Group GMP & T Cell Therapy, Deutsches Krebsforschungszentrum (DKFZ), Heidelberg, Germany
[14]Medical Faculty, University Hospital Carl Gustav Carus, NCT/UCC Section Medical Systems Biology, TU Dresden, Dresden, Germany
[15]Division of Experimental Hematology, Deutsches Krebsforschungszentrum (DKFZ) and DKFZ-ZMBH Alliance, Heidelberg, Germany
[16]Computational Oncology, Molecular Precision Oncology Program, National Center for Tumor Diseases (NCT) Heidelberg and Deutsches Krebsforschungszentrum (DKFZ), Heidelberg, Germany
[17]German Cancer Consortium (DKTK), Heidelberg, Germany
[18]Medical Department 1, University Hospital Carl Gustav Carus, TU Dresden, Dresden, Germany
[19]Charité-Universitätsmedizin Berlin, Corporate Member of Freie Universität Berlin, Humboldt-Universität zu Berlin, Department of Hematology, Oncology and Cancer Immunology, Berlin, Germany
[20]Molecular Medicine Partnership Unit, European Molecular Biology Laboratory, University of Heidelberg, Heidelberg, Germany
[21]Berlin Institute of Health (BIH) at Charité – Universitätsmedizin Berlin, Berlin, Germany
[22]Berlin Institute for Medical Systems Biology, Max Delbrück Center for Molecular Medicine in the Helmholtz Association, Berlin, Germany
[23]These authors contributed equally
[24]Lead contact
*Correspondence: a.trumpp@dkfz.de (A.T.), vkuchroo@evergrande.hms.harvard.edu (V.K.K.), simon.haas@bih-charite.de (S.H.)
https://doi.org/10.1016/j.stem.2022.04.007

SUMMARY

Hematopoietic stem and progenitor cells (HSPCs) are responsible for the production of blood and immune cells. Throughout life, HSPCs acquire oncogenic aberrations that can cause hematological cancers. Although molecular programs maintaining stem cell integrity have been identified, safety mechanisms eliminating malignant HSPCs from the stem cell pool remain poorly characterized. Here, we show that HSPCs constitutively present antigens via major histocompatibility complex class II. The presentation of immunogenic antigens, as occurring during malignant transformation, triggers bidirectional interactions between HSPCs and antigen-specific CD4$^+$ T cells, causing stem cell proliferation, differentiation, and specific exhaustion of aberrant HSPCs. This immunosurveillance mechanism effectively eliminates transformed HSPCs from the hematopoietic system, thereby preventing leukemia onset. Together, our data reveal a bidirectional interaction between HSPCs and CD4$^+$ T cells, demonstrating that HSPCs are not only passive receivers of immunological signals but also actively engage in adaptive immune responses to safeguard the integrity of the stem cell pool.

 © 2022 Elsevier Inc.

INTRODUCTION

Hematopoietic stem and progenitor cells (HSPCs) are the ultimate source of blood and immune cells, including antigen-presenting cells (APCs) and T cells (Doulatov et al., 2012; Eaves, 2015). In contrast to mature cell types, HSPCs are multipotent, long lived, and self-renew. The acquisition of genomic aberrations in HSPCs constitutes a major threat to the hematopoietic system since genomic errors are passed on to daughter stem cells and eventually to the entire hematopoietic system, where they are maintained throughout life. In the elderly, the establishment of such clonally expanded populations carrying preleukemic mutations is a frequent event and associated with a high risk of malignant transformation to hematological cancers (Genovese et al., 2014; Jaiswal et al., 2014). To protect stem cells from damage induced by replicative stress and reactive oxygen species, HSPCs are maintained in a long-term quiescent and low metabolic state (van Galen et al., 2014; Walter et al., 2015; Ho et al., 2017). Although inflammatory signals released during infections activate HSPCs to propel blood production, excessive exposure to inflammation induces replicative stress causing DNA damage and stem cell exhaustion (Essers et al., 2009; Sato et al., 2009; Walter et al., 2015; Zhang et al., 2016; Takizawa et al., 2017). $CD4^+$ regulatory T cells (Tregs) have been suggested to establish an immune privileged niche in the bone marrow (BM) maintaining stem cell quiescence, presumably by protecting stem cells from replicative stress induced by inflammatory insults (Fujisaki et al., 2011; Hirata et al., 2018). Although several mechanisms have been described how stem cells are passively protected by their microenvironment to prevent the acquisition of damage, active safety mechanisms that specifically eliminate malignant HSPCs from the system remain unknown.

Professional APCs, such as B cells or mature dendritic cells (DCs), induce adaptive immune responses by presenting antigens via the major histocompatibility complex class II (MHC-II) to the T cell receptor of $CD4^+$ T cells (Neefjes et al., 2011; Roche and Furuta, 2015). Microenvironmental factors, the maturation state of APCs, and the expression of costimulatory molecules on APCs have been implicated in balancing immunogenic versus tolerogenic T cell responses (Wakkach et al., 2003; Goodnow et al., 2005; Jurewicz and Stern, 2019). Professional APCs constitutively express high levels of MHC-II (Steinman, 2007; Merad et al., 2013; Roche and Furuta, 2015), whereas immature or nonprofessional APCs acquire antigen presentation activity only upon exposure to inflammatory signals associated with MHC-II upregulation (Kambayashi and Laufer, 2014; Jakubzick et al., 2017). The majority of other cell types are typically devoid of MHC-II expression and are not capable of priming $CD4^+$ T cells. Despite several studies reporting that MHC-II might be expressed on immature cells of the hematopoietic system (Russell and van den Engh, 1979; Fitchen et al., 1981; Sieff et al., 1982; Szer et al., 1985), HSPCs have not been considered capable of actively interacting with the adaptive immune system. Moreover, a systematic understanding of the MHC-II expression patterns is lacking, and the functionality as well as the role of MHC-II-mediated antigen presentation in HSPCs during health and disease remains unexplored.

Here, we demonstrate that HSPCs constitutively present antigens via MHC-II. Upon presentation of immunogenic antigens, HSPCs directly interact with antigen-specific $CD4^+$ T cells, driving HSPC differentiation and extinction from the system. On the other hand, $CD4^+$ T cells are activated and subsequently adopt an immunoregulatory state preventing harmful proinflammatory BM responses. This immunosurveillance mechanism effectively suppresses leukemia onset upon malignant transformation of HSPCs.

RESULTS

Mouse HSPCs express the MHC-II antigen-presenting machinery

To systematically explore the expression patterns of the MHC-II antigen presentation machinery in the hematopoietic system, we performed a series of analyses. First, global transcriptome datasets of mouse multipotent HSPCs (LSKs, $Lin^-Sca1^+cKit^+$ cells) revealed high expressions of genes encoding MHC-II molecules (*H2-Aa*, *H2-Ab1*, and *H2-Eb1*), the related antigen loading machinery (*H2-Dma, H2-Dmb2*, *H2-Oa*, *H2-Ob*, and *Cd74*), and *Ciita*, the master regulator of MHC-II gene expression (Steimle et al., 1993, 1994; Figure 1A). Targeted transcriptional profiling confirmed that MHC-II genes were highly expressed in mouse hematopoietic stem cells (HSCs) and multipotent progenitors (MPPs) 1–4 (Cabezas-Wallscheid et al., 2014), together comprising the LSK compartment (Figure 1B). These genes were gradually downregulated upon transition to committed progenitors that comprise the $Lineage^-Sca\text{-}1^-c\text{-}Kit^+$ (LS^-K) compartment. To analyze MHC-II protein expression, we measured MHC-II surface expression levels across all major cell populations present in the mouse BM and spleen by flow cytometry (Figures 1C, 1D, S1A, and S1B). As expected, professional APCs expressed consistently high levels of MHC-II, nonprofessional APCs expressed MHC-II at heterogeneous levels, and non-APCs did not express MHC-II. Importantly, HSCs and MPPs showed prominent surface expression levels of MHC-II, which were gradually downregulated upon transition to committed progenitors of the LS^-K compartment, in line with our transcriptomic data. Notably, homeostatic levels of MHC-II molecules in HSCs and MPPs were only slightly lower as compared with professional APCs but significantly higher when compared with any other population examined, including macrophages (Figures 1C, 1D, S1A, and S1B). Transcript and protein levels of MHC-II genes were efficiently upregulated in HSCs *in vivo* upon administration of bacterial lipopolysaccharide (LPS), recombinant type-I interferon, the viral mimetic polyinosinic:polycytidylic acid (pI:C), or following viral infection with mouse cytomegalovirus (MCMV) (Figures 1C, 1D, and S1A–S1C). Stimulation by LPS or pI:C treatment of mice enhanced the expression of MHC-II surface levels on HSCs comparable to those observed in professional APCs but had only a negligible impact on non-APCs.

To unambiguously determine whether MHC-II expression marks HSCs with long-term self-renewal capacity, we separated lineage-depleted BM solely based on MHC-II surface expression, followed by transplantation into lethally irradiated mice (Figures 1E, 1F, S1D, and S1E). While MHC-II-negative BM cells were not capable of repopulating all hematopoietic

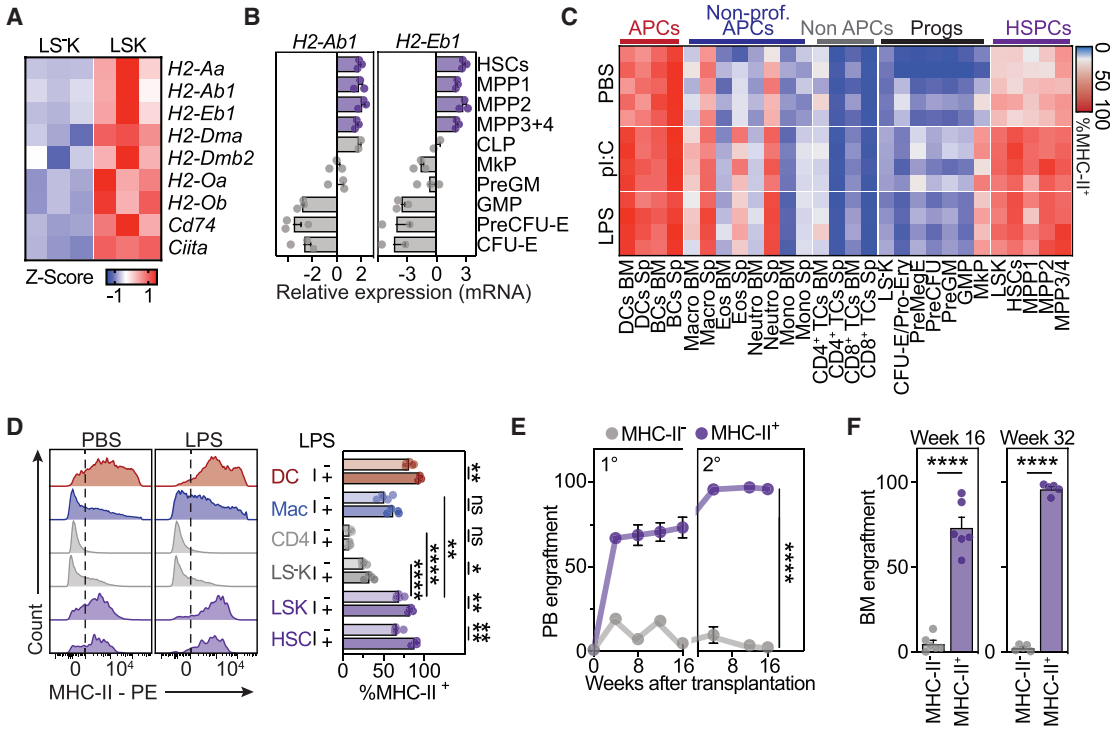

Figure 1. Mouse HSPCs express the MHC-II antigen presentation machinery

(A) *Z* scores of MHC-II antigen presentation machinery genes in mouse HSCs and MPPs (LSK) and progenitors (LS^{-}K) derived from RNA-seq data (Klimmeck et al., 2014), n = 3.

(B) Relative gene expression of MHC-II genes across bone marrow (BM) populations measured by qPCR, n = 2–3.

(C) Heatmap summarizing MHC-II surface measurements for BM and spleen (Sp) populations by flow cytometry at homeostasis or 24 h post pI:C or LPS treatment.

(D) Representative histograms (left) and quantification (right) of MHC-II surface expression as in (C), n = 4–5.

(E and F) Transplantation experiments of MHC-II$^{+/-}$ BM populations, n = 4–6.

(E) Peripheral blood (PB) chimerism, n = 4–6.

(F) BM chimerism at the endpoint of primary (left) and secondary (right) transplantations, n = 4–6.

Individual values are shown in (A) and (C), means and SEM are depicted otherwise. No significance = ns, $p < 0.05$*, $p < 0.01$**, $p < 0.001$***, $p < 0.0001$****. Two-way ANOVA was performed in (D) as discovery test, followed by a paired two-tailed t test. If not stated otherwise, unpaired two-tailed t tests were performed as post hoc tests. Two-way ANOVA was performed in (E).

See also Figure S1.

lineages efficiently, MHC-II-positive BM cells reconstituted hematopoiesis long term, demonstrating that MHC-II surface expression is an explicit feature of self-renewal capacity and therefore marks all functional HSCs.

Mouse HSPCs present antigens via MHC-II

To determine whether mouse HSPCs are capable of presenting antigens via MHC-II, we made use of the Y-Ae antibody that recognizes the MHC-II-derived Eα peptide$_{52-68}$ when presented in the context of MHC-II I-A^{b} haplotype (Murphy et al., 1989; Rudensky et al., 1991). Accordingly, in C57BL/6 mice that display the I-A^{b} haplotype but lack expression of Eα, exogenous Eα peptide can be used as foreign antigen to characterize antigen presentation capacities of cell populations *ex vivo*. While professional APCs efficiently presented the Eα peptide via MHC-II and non-APCs failed to do so, HSPCs presented MHC-II-restricted peptides efficiently, suggesting that HSPCs can present exogenous peptides *ex vivo* (Figure 2A). In support of this, HSPCs efficiently incorporated and processed exogenously administered BODIPY-conjugated DQ-ovalbumin (DQ-OVA), a self-quenched conjugate that exhibits fluorescence upon cleavage, *ex vivo* and *in vivo* (Figures S1F–S1H).

To investigate whether HSPCs of naive mice present self-antigens via MHC-II *in vivo*, we crossed BALB/c mice, which express Eα but exhibit the I-A^{d} haplotype, to C57BL/6 mice (I-A^{b}, Eα-negative). In mice of the F1 generation, MHC-II-mediated self-antigen presentation can be assessed by the Y-Ae antibody, due to the expression of Eα in the presence of MHC-II molecules with I-A^{b} haplotype (Henri et al., 2010; Figure S1I). In line with previous reports, professional APCs displayed efficient MHC-II-mediated presentation of Eα during homeostasis, and upon LPS treatment *in vivo*, macrophages did not present Eα at homeostasis but acquired strong antigen presentation capacity upon LPS treatment and non-APCs showed no or highly restricted antigen-presenting activity (Kambayashi and Laufer, 2014; Jakubzick et al., 2017; Figures 2B, 2C, and S1J). Importantly, HSCs and MPPs exhibited significant antigen presentation of Eα at homeostasis and efficiently increased

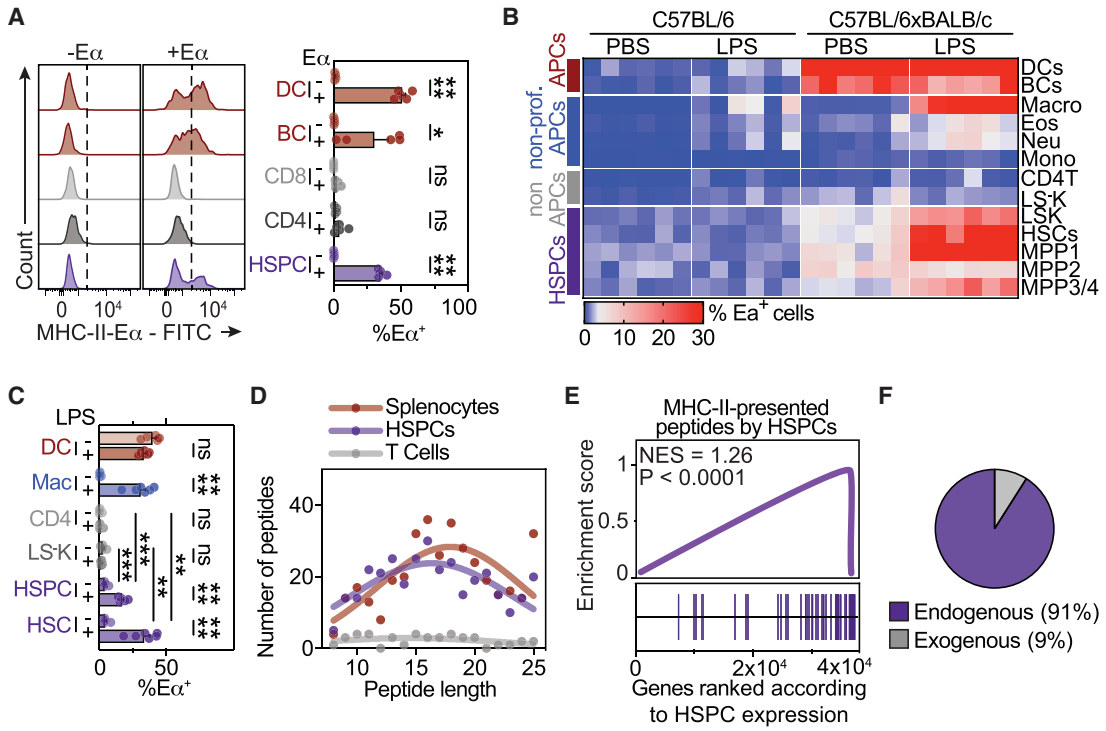

Figure 2. Mouse HSPCs present self-antigens via MHC-II

(A) *Ex vivo* antigen presentation assay. Representative histograms (left) and quantification (right), n = 4.

(B and C) *In vivo* antigen presentation assay, n = 6. (B) Heatmap summarizing the percentage of Eα presenting cells in C57BL/6 × BALB/c mice and control C57BL/6 mice. (C) Quantification of selected populations in C57BL/6 × BALB/c.

(D–F) Mass spectrometry analyses of peptides recovered from MHC-II of indicated populations. (D) MHC-II-eluted peptide size distribution. (E) Gene set enrichment analysis (GSEA) of presented peptides related to their gene expression in HSPCs. (F) MHC-II-derived peptides in HSPCs that are transcribed (endogenous) or not transcribed (exogenous) within HSPCs based on a threshold of 100 RPKM.

Individual values are shown in (B) and (D), means and SEM are depicted otherwise. No significance = ns, $p < 0.05$*, $p < 0.01$**, $p < 0.001$***, $p < 0.0001$****. One- (A) or two-way ANOVA (C) were performed as discovery tests. Paired two-tailed t test was performed in (C). If not stated otherwise, unpaired two-tailed t tests were performed as post hoc tests.

See also Figure S1.

antigen-presenting capacity upon LPS treatment in an MHC-II-restricted manner, suggesting that HSPCs constantly present self-peptides via MHC-II in naive mice (Figures 2B, 2C, and S1J).

To identify antigens presented by HSPCs, we performed immunoprecipitation of MHC-II molecules from HSPCs of naive mice, followed by peptide elution and mass spectrometry (Figures 2D and 2E). We also included T cells and splenocytes, serving as negative and positive control of APCs, respectively. MHC-II-eluted peptides from HSPCs resembled those from splenocytes in number and length distribution and considerably outnumbered peptides eluted from non-APCs (Figure 2D). The evaluation of detected peptides confirmed that predominantly self-peptides are presented by HSPCs in naive mice (Figures 2E and 2F; Table S1). Together, these data demonstrate that HSPCs constitutively present self-antigens via MHC-II at homeostasis and further increase antigen presentation upon inflammation.

Antigen-presenting HSPCs engage in bidirectional interactions with antigen-specific CD4$^+$ T cells

The main feature of APCs is the antigen-specific activation of CD4$^+$ T cells. To study whether HSPCs can interact with CD4$^+$ T cells in an antigen-specific manner, we made use of OT-II and 2D2 mice that express transgenic T cell receptors specifically recognizing the chicken ovalbumin ($OVA_{323-339}$) or myelin oligodendrocyte glycoprotein (MOG_{35-55}) peptides, respectively, when presented by MHC-II (Barnden et al., 1998; Bettelli et al., 2003). In cocultures with multipotent HSPCs (LSKs), naive antigen-specific CD4$^+$ T cells were efficiently activated and proliferated specifically in the presence of the respective peptides (Figures 3A, 3B, and S2A–S2D). Notably, all populations of the LSK compartment, including HSCs and MPPs1-4 induced antigen-specific CD4$^+$ T cell responses (Figure 3C). Since these populations also express similar levels of MHC-II and exhibit comparable presentation of endogenous antigens *in vivo* (see above), we used LSK cells in the majority of functional experiments that characterize antigen presentation of mouse multipotent HSPCs. Importantly, blocking MHC-II abrogated HSPC-mediated activation of CD4$^+$ T cells, demonstrating that antigen-specific CD4$^+$ T cell activation is MHC-II dependent (Figure S2E). While HSPCs efficiently activated CD4$^+$ and CD8$^+$ T cells in the presence of processed peptides, they were also able to present antigens derived from OVA protein, albeit to a lesser extent if compared with DCs (Figures S2F and S2G).

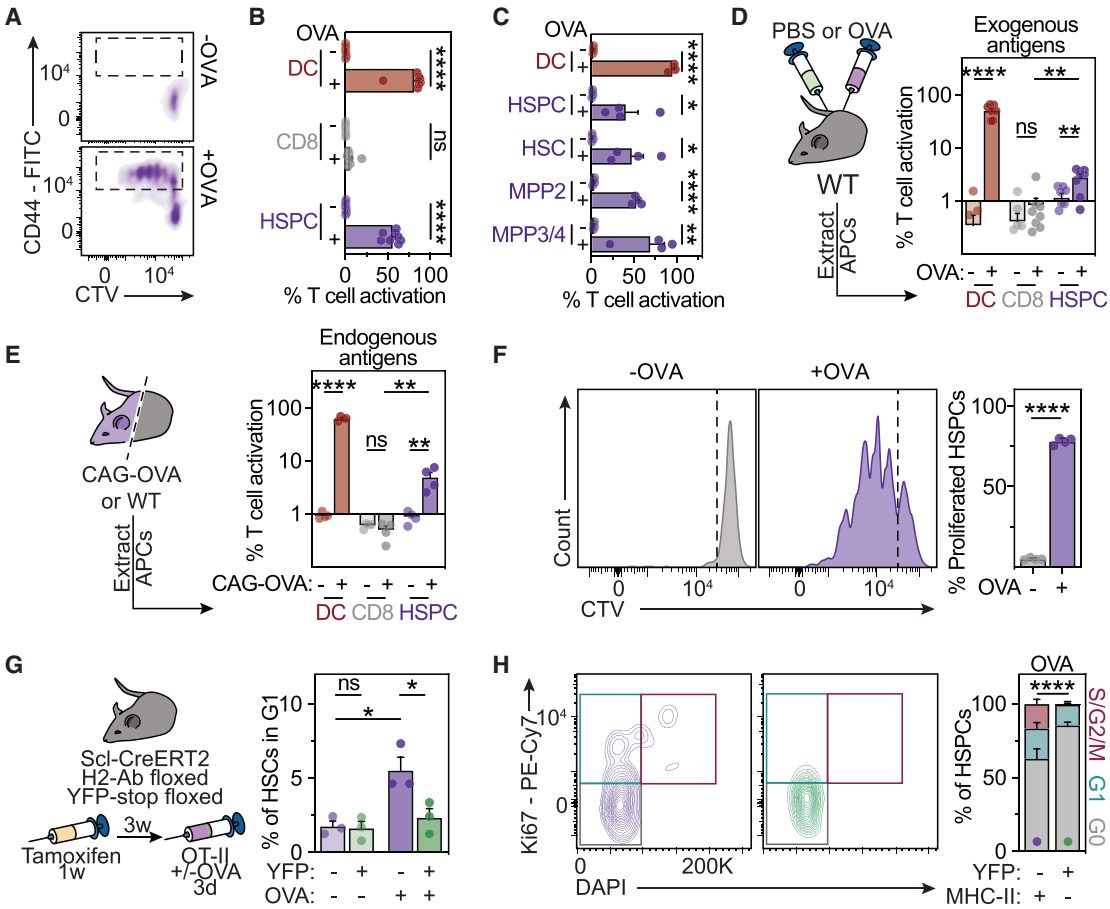

Figure 3. MHC-II mediates an antigen-specific bidirectional interaction between HSPCs and CD4$^+$ T cells

(A and B) HSPCs activate naive OT-II CD4$^+$ T cells in coculture assays, n = 8. (A) Representative histograms of CD44 expression and cell trace violet (CTV). (B) Quantification of T cell activation.

(C) T cell activation assays for different HSPC subpopulations (2.5 × 10^3 cells) as in (A), n = 4.

(D) *In vivo* antigen presentation assay for exogenous antigens. Experimental approach (left), quantification of T cell activation (right), n = 8.

(E) *In vivo* antigen presentation assay for endogenous antigens. Experimental approach (left), quantification of T cell activation (right), n = 4.

(F) Antigen presentation impacts on HSPC proliferation in coculture assays with naive OT-II CD4$^+$ T cells (see STAR Methods). Representative plots (left) and quantification (right), n = 4.

(G and H) *In vivo* antigen-specific HSPC-T cell interaction promotes HSPC cell cycle entry in a Scl-CreERT2 H2-Ab floxed YFP-stop floxed mouse model. (G) Experimental scheme (left) and cell cycle analyses (right). (H) Representative plots (left) and cell cycle analysis (right) of YFP$^+$MHC-II$^-$ or YFP$^-$MHC-II$^+$ HSPCs from Cre$^+$ mice, n = 5.

Means and SEM are depicted. No significance = ns, $p < 0.05$*, $p < 0.01$**, $p < 0.001$***, $p < 0.0001$****. One- (B and C) or two-way ANOVA (D, E, G, and H) were performed as discovery tests. Paired two-tailed t test was performed in (G). If not stated otherwise, unpaired two-tailed t tests were performed as post hoc tests. See also Figure S2.

However, LPS-induced inflammatory signals significantly enhanced the HSPC-mediated antigen-specific activation of T cells.

To determine whether HSPCs are capable of incorporating, processing, and presenting exogenous antigens *in vivo*, we administered OVA protein to mice. Indeed, HSPCs isolated from OVA-injected mice were able to activate antigen-specific OT-II CD4$^+$ T cells *ex vivo* (Figure 3D), indicating their capability to process and present exogenous antigens *in vivo*. To confirm whether HSPCs were also able to present endogenous antigens, we cocultured HSPCs from wild-type or ovalbumin-expressing mice (CAG-OVA) with OT-II T cells. Indeed, OT-II T cells were specifically activated in the presence of HSPCs expressing OVA endogenously, albeit to a lesser extent if compared with mature DCs (Figure 3E). Together, these experiments suggest that HSPCs are capable of activating CD4$^+$ T cells upon presentation of both, endogenous and exogenous antigens via MHC-II.

Next, we investigated the impact of MHC-II-mediated antigen presentation on HSPCs. In cocultures, antigen-specific interactions with naive CD4$^+$ T cells resulted in substantial proliferation of HSPCs (Figures 3F and S2H). Moreover, transwell assays demonstrated that direct contact between HSPCs and CD4$^+$ T cell cells is required for full cell cycle activation of HSPCs *ex vivo* (Figures S2I and S2J). To evaluate the mechanistic role of MHC-II in HSPC-T cell interactions *in vivo*, we generated mice carrying a tamoxifen-inducible recombinase CreERT2

under the control of the HSPC-specific SCL promoter, a loxP-flanked MHC-II allele (*H2-Ab*) and a loxP-flanked STOP sequence followed by the enhanced yellow fluorescent protein (YFP) (Figure 3G; see STAR Methods). This enabled an efficient conditional deletion of MHC-II in HSPCs and their progeny (Figures S2K and S2L). Cotransfer of OVA-specific OT-II cells into tamoxifen-treated mice, followed by OVA immunization resulted in specific cell cycle induction of HSPCs that maintained physiological MHC-II levels, whereas MHC-II-deficient HSPCs from the same mice did not respond to OVA treatment (Figures 3G and 3H). Together, these observations demonstrate that presentation of immunogenic antigens via MHC-II by HSPCs mediates bidirectional interactions with antigen-specific $CD4^+$ T cells, resulting in simultaneous activation of stem and T cells.

Sustained antigen presentation drives differentiation and elimination of HSPCs from the stem cell pool

To investigate the physiological relevance of our findings, we modeled the long-term consequences of sustained presentation of immunogenic antigens by HSPCs as occurring during chronic infections or malignant transformation. For this purpose, we generated mice with chimeric hematopoietic systems by co-transplantation of equal numbers of wild-type HSPCs and CAG-OVA HSPCs, constitutively presenting OVA, into lethally irradiated congenic mice (Figure 4A). In the absence of antigen-specific $CD4^+$ T cells, this resulted in a stable 50:50 chimerism of the two hematopoietic systems throughout primary and secondary transplantation, suggesting that the presentation of antigens in the absence of antigen-specific $CD4^+$ T cells does not affect hematopoiesis (Figure 4B). In contrast, upon cotransfer of OVA-specific OT-II $CD4^+$ T cells at the beginning of the primary transplantation (d0), OVA-expressing HSPCs were immediately removed from the system, resulting in a complete and specific engraftment failure of stem cells presenting the T cell-recognized antigen (Figures 4B and 4C). If OT-II $CD4^+$ T cells were cotransferred after stable engraftment of the two hematopoietic systems (d60 post-transplantation), the chimerism was kept stable initially but started dropping upon secondary transplantation. Importantly, also in this setting, antigen-presenting HSPCs were efficiently decreased and eliminated after primary and secondary transplantations, respectively.

Although antigen-specific $CD4^+$ T cells strongly expanded and accumulated in the BM during stem cell exhaustion, antigen-specific $CD8^+$ T cells were not detected (Figures 4D, S2M, and S2N), suggesting that the elimination of antigen-presenting HSPCs was mediated by direct $CD4^+$ T cell interactions and not by secondary activation of cytotoxic $CD8^+$ T cells. Of note, loss of OVA-presenting HSPCs was associated with an increased myeloid-biased differentiation (Figure 4E). To determine whether differentiation is the main cause of elimination of antigen-presenting stem cells, we first investigated the impact of antigen presentation on HSPCs differentiation. In cocultures, antigen-specific interactions with $CD4^+$ T cells induced rapid differentiation of HSPCs into the myeloid lineage, associated with loss of *in vivo* stem cell potential as measured by BM transplantations (Figures 4F–4I and S2O). Gene expression analyses confirmed the upregulation of differentiation programs in HSPCs and their progeny (Figure S2P). In line with this, cotransfer of OVA-loaded HSPCs with OVA-specific $CD4^+$ T cells into mice resulted in rapid differentiation of HSPCs *in vivo* (Figures 4J and 4K). Finally, transwell assays demonstrated that direct HSPC-$CD4^+$ T cell interactions are required to effectively drive HSPC differentiation, whereas additional indirect effects mediated by the establishment of cytokine gradients are likely to contribute to the observed effect as well (Figure S2Q). Together, these data suggest that direct interactions with antigen-specific $CD4^+$ T cells drive differentiation and exhaustion of HSPCs that present the cognate immunogenic antigens via MHC-II, thereby irreversibly removing them from the system while leaving unrecognized self-antigen-presenting HSPCs unaffected.

Antigen-specific HSPC-$CD4^+$ T cell interactions promote an immunoregulatory state

Inflammatory signals, such as those released during proinflammatory T cell responses, induce systemic HSPC proliferation (Essers et al., 2009; Baldridge et al., 2010; Walter et al., 2015; (Haas et al., 2015)). However, antigen presentation by HSPCs resulted in the specific activation and exhaustion of stem cells that actively present immunogenic antigens while leaving self-antigen-presenting HSPCs unaffected (see above), suggesting that HSPC-mediated T cell activation occurs in the absence of global proinflammatory BM responses. Since naive $CD4^+$ T cells can be polarized into proinflammatory or immunosuppressive T helper subsets depending on the properties of the APC and environmental factors (Zhu and Paul, 2010), we investigated the exact nature of HSPC-induced T cell polarization.

First, we characterized the APC properties of HSPCs. Gene expression analyses of HSPCs revealed low-to-intermediate expression of classical costimulatory molecules but high surface presentation of the coinhibitory molecule PD-L1 (Figures S3A and S3B). Moreover, the most highly expressed cytokine genes in HSPCs are *Ebi3* and *Il12a* (Figure S3C), forming together the suppressive cytokine IL-35 (Collison et al., 2007, 2010). Upon engagement with antigen-specific $CD4^+$ T cells, HSPCs further upregulated PD-L1, acquired features of myeloid-derived suppressor cells, and expressed high levels of the immunoregulatory cytokines IL-10 and IL-27 (Figures S3D–S3H). Since high expression of immunoregulatory cytokines and coinhibitory receptors by APCs are associated with the promotion of anti-inflammatory or immunoregulatory responses (Ness et al., 2021), we investigated whether antigen presentation by HSPCs might polarize $CD4^+$ T cells to an immunoregulatory state. Indeed, in contrast to $CD4^+$ T cells activated by other APCs, $CD4^+$ T cells activated by HSPCs acquired a unique state, characterized by high surface expression of coinhibitory molecules, such as PD-L1 (Figures S4A and S4B). This was also the case for $CD4^+$ T cells activated by highly purified HSCs and MPP populations (Figure S4C). Global transcriptomic comparisons of $CD4^+$ T cells activated by HSPCs, in the following termed T_{HSCs}, with $CD4^+$ T cells activated by conventional DCs (T_{DCs}) confirmed that they acquired fundamentally distinct transcriptomic states, with T_{HSCs} adopting an immunoregulatory and anti-inflammatory phenotype (Figures 5A and 5B). Of note, the expression of the signature transcription factor of Tregs, *Foxp3*, remained absent upon HSPC-mediated T cell activation (Figure S4D). In contrast, an upregulation of the transcription factors *c-Maf* and *Prdm1* was observed, which act as master regulators of type 1 regulatory (Tr1) T cell differentiation and mediate the

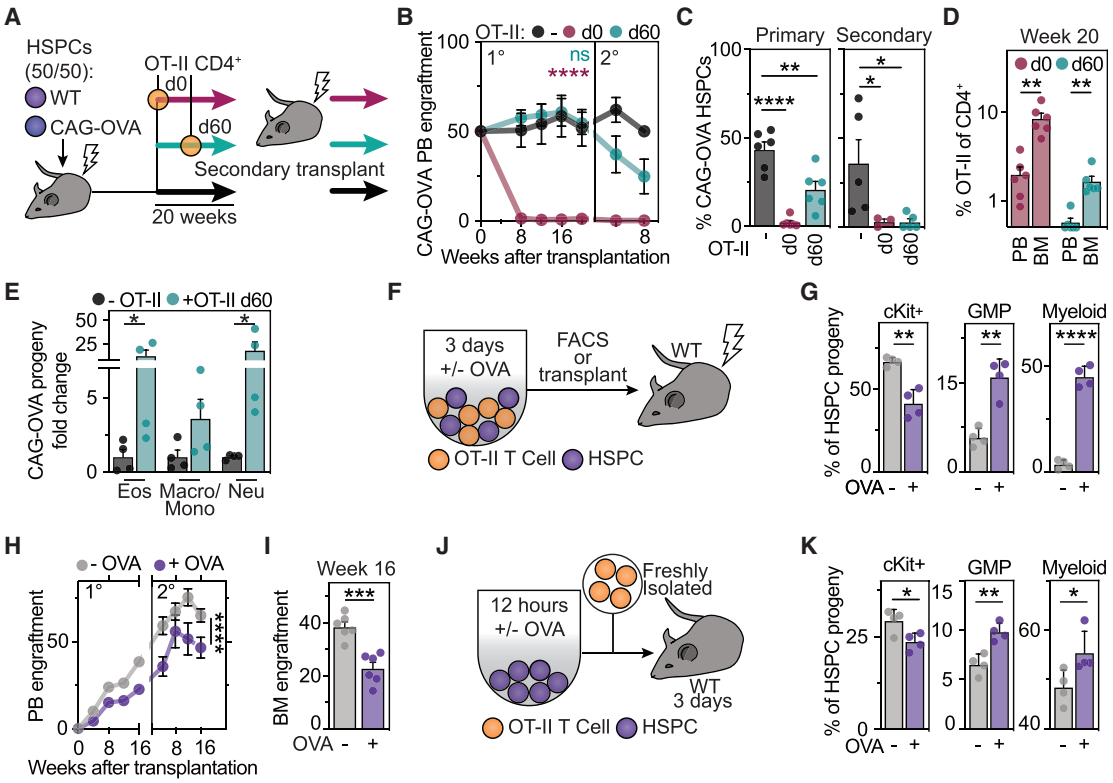

Figure 4. Sustained presentation of immunogenic antigens drives differentiation and exhaustion of HSPCs

(A–E) Sustained *in vivo* interactions of antigen-presenting HSPCs and antigen-specific CD4$^+$ T cells trigger HSPC differentiation and exhaustion.

(A) Experimental scheme: cotransplantations of CAG-OVA and WT HSPCs with or without OT-II CD4$^+$ T cells.

(B) Percentage of CAG-OVA progeny in the blood of recipient mice, n = 4–6.

(C) BM chimerism at the endpoints of primary (left) and secondary (right) transplantations, n = 4–6.

(D) Percentage of OT-II T cells of total CD4$^+$ T cells in recipient mice (week 20), n = 6.

(E) Lineage-output upon HSPC-T cell interactions *in vivo*. Percentage of CAG-OVA HSPC-derived progeny 20 weeks after transplantation, n = 4.

(F–I) Impact of antigen presentation on HSPC differentiation.

(F) Experimental scheme. Cocultures between HSPCs and OT-II T cells were analyzed by flow cytometry (G) or transplanted into lethally irradiated mice (H) and (I).

(G) Indicated populations derived from transplanted HSPCs were quantified, n = 4.

(H) PB engraftment, n = 6.

(I) BM engraftment at week 16, n = 6.

(J and K) *In vivo* impact of antigen presentation on HSPCs.

(J) Experimental scheme. OVA-loaded HSPCs were cotransferred with naive OT-II CD4$^+$ T cells.

(K) Indicated populations were quantified 3 days post-transfer.

Means and SEM are depicted. No significance = ns, $p < 0.05$*, $p < 0.01$**, $p < 0.001$***, $p < 0.0001$****. One-way (C, D, and E) and two-way (B and H) ANOVA was performed. If not stated otherwise, unpaired two-tailed t tests were performed as post hoc tests.

See also Figure S2.

transcriptional induction of coinhibitory gene modules in T cells (Chihara et al., 2018; Zhang et al., 2020; Figures 5B,S4D, and S4G). In line with this, T_{HSCs} upregulated robust and sustained expressions of the immune suppressive cytokine IL-10 and a coinhibitory gene module comprising the coinhibitory molecules PD-1 (*Pdcd1*), PD-L1 (*Cd274*), LAG3 (*Lag3*), and TIM3 (*Havcr2*) on the mRNA and protein level (Figures 5C and S4D–S4F). The expression of coinhibitory molecules and signature Tr1 transcription factors in T_{HSCs} remained elevated upon resting, antigen-dependent, or antigen-independent restimulation and exposure to inflammatory molecules, suggesting that the regulatory phenotype is not due to a transient activation state but rather reflects a stable state linked to differentiation (Figures S4G–S4J).

To evaluate whether T_{HSCs} acquired a functionally suppressive phenotype *ex vivo*, we performed suppression assays using canonical Tregs as control (Figures 5D–5G). In contrast to T_{DCs}, T_{HSCs} efficiently suppressed CD4$^+$ and CD8$^+$ T cell responses in an antigen-dependent and antigen-independent manner (Figures 5D–5H). Moreover, T_{HSCs} reduced the cytotoxic activity of CD8$^+$ T cells and supported macrophage polarization to an anti-inflammatory M2 state (Figures 5I and 5J). Mechanistically, both the capacity of T_{HSCs} to suppress bystander T cells and to polarize macrophages to an M2 state was, at least partly, driven by IL-10 (Figures 5J and 5K), which is upregulated both in HSPCs and CD4$^+$ T cells upon bidirectional interactions (see above). Adoptive transfers of T_{HSCs} into mice effectively suppressed the response of naive OT-II T cells to OVA

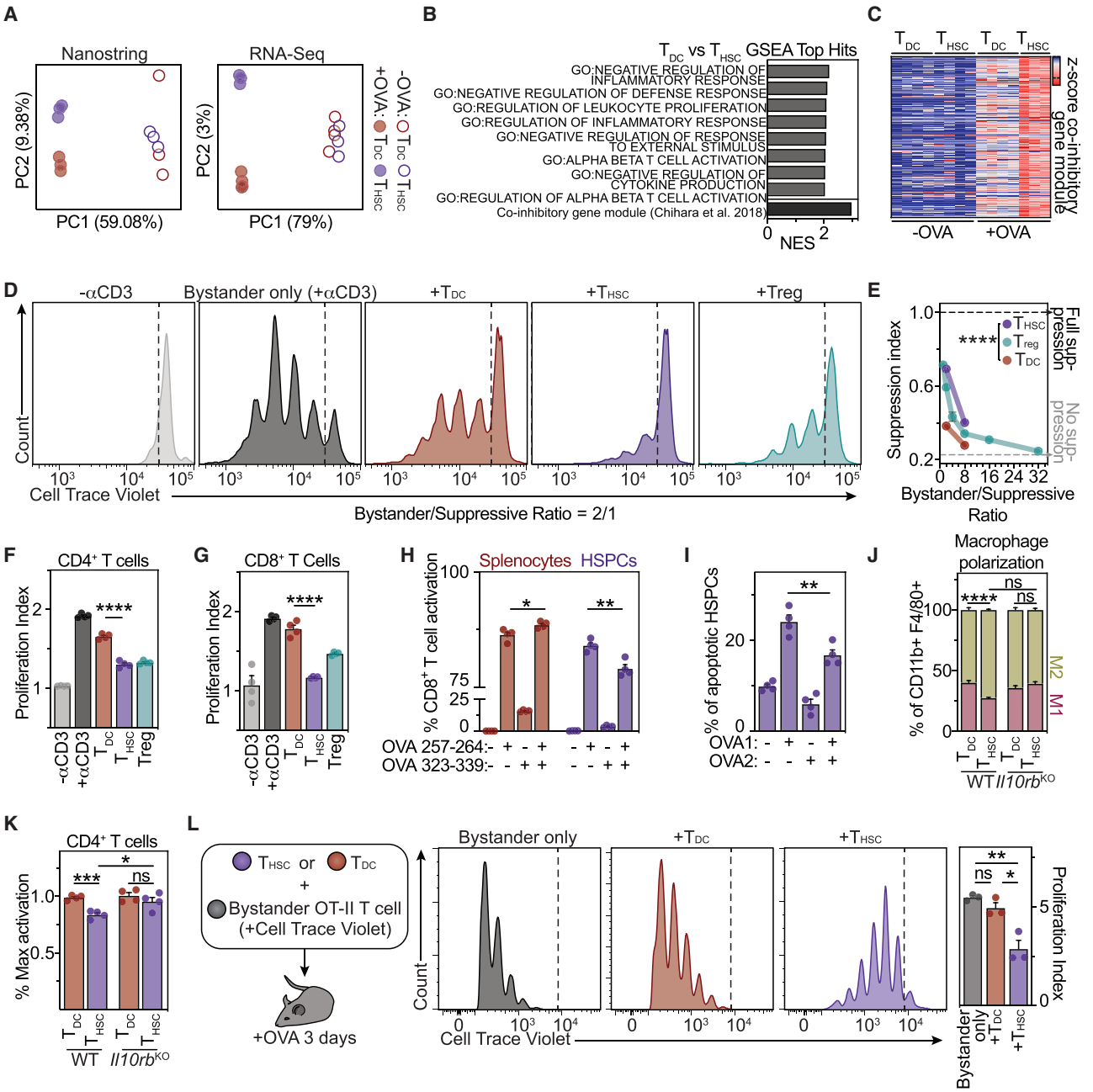

Figure 5. HSPC-mediated antigen presentation induces a suppressive phenotype in CD4⁺ T cells

(A) Principle component analyses (PCA) of Nanostring (left) and RNA-seq (right) gene expression of OT-II CD4⁺ T cells activated by HSPCs (T_{HSCs}) or dendritic cells (T_{DCs}), n = 3–4.

(B) Top T_{HSC}-enriched gene sets of gene set enrichment analyses (GSEA) of RNA-seq data from (A), comparing T_{HSCs} and T_{DCs}.

(C) Heatmap representing *Z* scored expressions of coinhibitory module genes (Chihara et al., 2018).

(D–F and K) *Ex vivo* CD4⁺ T cell suppression assays. (D) Representative plots for the 1:2 suppressive/bystander naive CD4⁺ T cell condition. (E) Suppression index for different bystander/suppressive ratios, n = 4. (F) Proliferation index of responder CD4⁺ T cells for the 1:2 ratio, n = 4. (K) follows the same methodology as (D)–(F).

(G) *Ex vivo* CD8⁺ T cell suppression assay, n = 4.

(H and I) *Ex vivo* CD8⁺ T cell activation (H) and annexin V cytotoxicity assay (I), n = 4. OVA1: ovalbumin 257–264, OVA2: ovalbumin 323–339.

(J) *Ex vivo* macrophage polarization assay, n = 4.

(K) Role of IL-10 in T_{HSC}-mediated suppression. Activation of WT (left) or *Il10rb*$^{-/-}$ (right) bystander T cells in the presence of T_{HSCs} or T_{DCs} in a 1:2 suppressive:bystander ratio, n = 4.

(legend continued on next page)

immunizations, demonstrating the *in vivo* capacity of T_{HSCs} to dampen the immune system (Figure 5L).

In line with our *ex vivo* results, upon sustained interactions with CAG-OVA HSPCs *in vivo*, antigen-specific $CD4^+$ T cells acquired a PD-L1 high phenotype (Figure S4K). Both antigen-specific $CD4^+$ T cells and the CAG-OVA HSPC-derived BM cells of mice in which HSPC-mediated antigen presentation occurred adopted a functionally suppressive phenotype, confirming that sustained antigen presentation by HSPCs causes an overall immunoregulatory BM response *in vivo* (Figures S4L and S4M).

Together, these findings demonstrate that antigen presentation by HSPCs to $CD4^+$ T cells triggers HSPC and T cell activation while promoting an immunoregulatory environment to avoid harmful proinflammatory responses in the BM.

Human HSPCs are antigen-presenting cells

In order to investigate whether our findings in the mouse system can be translated to humans, we first analyzed bulk and single-cell transcriptome datasets of human HSPCs (Novershtern et al., 2011; Hay et al., 2018; Pellin et al., 2019). These analyses revealed high expressions of genes encoding MHC-II (e.g., *HLA-DRA*, *HLA-DRB*) and the machinery related to antigen presentation via MHC-II (e.g., *HLA-DMA*, *HLA-DMB*, and *CD74*) in HSCs and MPPs (Figures 6A, S5A, and S5B). Although the expression of MHC-II and its antigen-presenting machinery was maintained throughout commitment of HSCs to lineages with APC function (DC, B cell, and monocyte/macrophage lineages), it was gradually downregulated upon commitment to all other lineages (neutrophil, eosinophil/basophil/mast cell, erythroid, and megakaryocytic lineages). We next performed a flow cytometric characterization of the cell surface expression of the MHC-II molecule HLA-DR across major hematopoietic compartments of the BM from healthy donors. The results accurately recapitulated our findings from the mouse system, with no expression of HLA-DR in non-APCs, high expression in professional APCs, and robust, albeit slightly lower expression in HSPCs and early progenitors of the $CD34^+$ compartment (Figures 6B, 6C, and S5C). To confirm that MHC-II marks human HSCs with long-term self-renewal capacity, we transplanted human BM, separated solely based on HLA-DR expression, into sublethally irradiated immunodeficient mice (Figure 6D). Notably, HLA-DR-positive BM cells gave rise to significantly higher levels of human multilineage engraftment compared with HLA-DR-negative BM20 weeks post-transplant, suggesting that functional HSC activity is associated with MHC-II expression (Figure 6E).

To investigate whether human HSPCs are capable of presenting antigens via MHC-II, we made use of CytoStim, an antibody-based reagent that cross-links MHC-II of APCs with the T cell receptor of $CD4^+$ T cells, resulting in T cell activation. As expected, addition of CytoStim resulted in efficient activation of $CD4^+$ T cells in cocultures with professional APCs but had little or no effect in cocultures with non-APCs (Figures 6F and 6G). In contrast, addition of CytoStim to cocultures of $CD34^+$ HSPCs and $CD4^+$ T cells resulted in efficient T cell activation, which was comparable with DC-mediated T cell activation. To determine whether human HSPCs can activate $CD4^+$ T cells in an antigen-dependent manner, we made use of a pool of peptides frequently recognized by a small subset of antigen-experienced $CD4^+$ T cells (Figure 6H). Notably, the $CD34^+$ cells that were used for functional assays have been purely sorted, displaying an neglectable amount of immature DCs and B cells (Figure S5D). According to our previous observations, APCs and HSPCs comparably activated antigen-specific $CD4^+$ T cells . Of note, similar to their mouse counterparts, human $CD4^+$ T cells activated by human $CD34^+$ HSPCs acquired an immunoregulatory phenotype associated with upregulation of coinhibitory molecules, such as LAG3, PD-L1, and TIM3, as well as increased expression of the *IL10* gene and Tr1-associated transcription factors, suggesting a conserved mechanism from mouse to human (Figures 6I–6K). Collectively, these data suggest that human HSPCs, similar to their mouse counterparts, act as APCs capable of interacting with $CD4^+$ T cells via MHC-II.

MHC-II-mediated antigen presentation is associated with a stem-like state in AML

Acute myeloid leukemia (AML) is an aggressive hematological cancer characterized by the accumulation of immature blasts that originate from HSCs or myeloid progenitors. MHC-II has been described to be expressed in a heterogeneous manner in AML (Miale et al., 1982; Newman et al., 1983), and its deregulation has been linked to relapse after allogeneic stem cell transplantation (Christopher et al., 2018; Toffalori et al., 2019). However, neither a rationale for MHC-II expression heterogeneity nor a link to APC capacity and clinical or biological features of AMLs has been established (Miale et al., 1982; Mutis et al., 1997, 1998; Costello et al., 1999; Berlin et al., 2015). In line with our previous findings in the healthy hematopoietic system, transcriptomic analyses of 523 leukemia samples of AML patients revealed that high expressions of the MHC-II antigen presentation machinery is associated with a transcriptomic state of stemness (Pölönen et al., 2019; Figure 7A). In accordance with this, flow cytometric analyses of 63 AML patients confirmed that high HLA-DR (MHC-II) surface expression identifies patients with stem-like or monocyte-like AMLs and marks immature stem-like populations within the leukemic blast hierarchy of individual patients (Figures 7B, 7C, and S5E–S5G). To determine whether a stem-like state in human AML is indeed associated with functional APC capacities, we screened 23 human AML cell lines and categorized them based on their immunophenotype into stem- or mature-like (Figures S5H and S5I). In line with our observations in primary AMLs, stem-like AML cell lines expressed higher HLA-DR levels, displayed higher $CD4^+$ T cell activation and immunosuppressive polarization capacities, and underwent myeloid differentiation upon antigen presentation, suggesting that the above-described bidirectional

(L) *In vivo* suppression assay. Representative plots (left) and quantification of bystander T cell proliferation (right), n = 3.

Individual values are shown in (A) and (C), means and SEM are depicted otherwise. No significance = ns, $p < 0.05$*, $p < 0.01$**, $p < 0.001$***, $p < 0.0001$****. One- (F, G, H, I, and L) or two-way ANOVA (K) were performed as discovery test. Two-way ANOVA was performed in (E) and (J). if not stated otherwise, unpaired two-tailed t tests were performed as post hoc tests.

See also Figures S3 and S4.

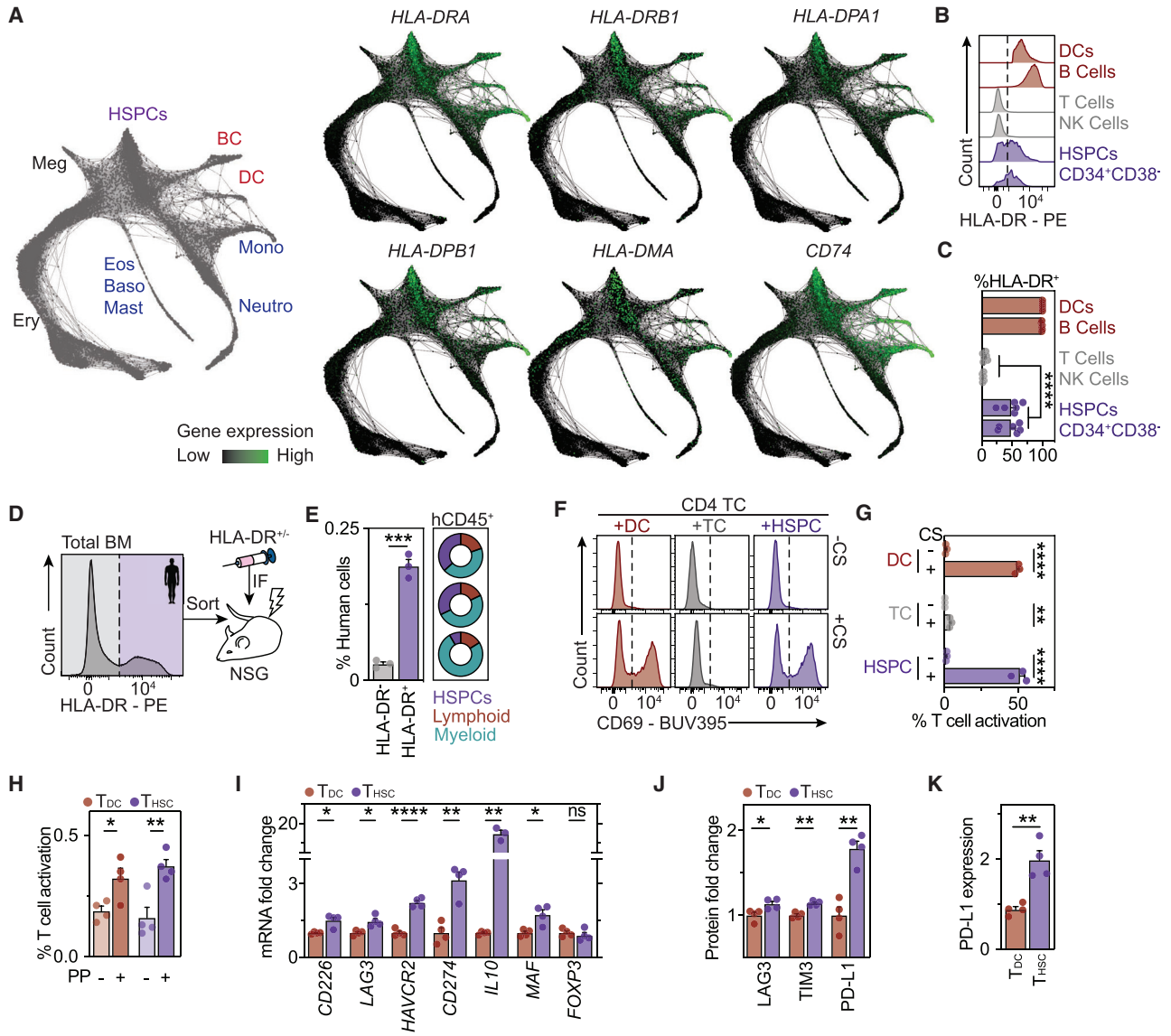

Figure 6. Human HSPCs act as antigen-presenting cells

(A) SPRING plots of human HSPC differentiation trajectories from scRNA-RNA-seq data (Pellin et al., 2019). Lineage annotation (left) and MHC-II gene expression (right).

(B) Representative plots of HLA-DR expression in human BM aspirates, n = 6.

(C) Quantification of HLA-DR$^+$ expression from (B).

(D) Experimental scheme for xenotransplantations.

(E) Quantification of human CD45$^+$ cells in the BM (left) and multilineage engraftment (right) in xenotransplantations. Donut plots depict myeloid, lymphoid, and HSPC percentages for every donor, n = 3.

(F–H) Human CD4$^+$ T cell activation assays using CytoStim (CS, F and G) or an MHC-II-restricted peptide pool (PP, H). Representative plots (F) and quantification of T cell activation (G and H), n = 3–4.

(I) qPCR analyses of CD4$^+$ T cells activated by HSPCs (T_{HSCs}) or dendritic cells (DCs) (T_{DCs}) in the presence of CytoStim as in (F), n = 4.

(J and K) Surface protein expression in T_{HSCs} and T_{DCs}, n = 4.

Means and SEM are depicted in all bar plots. No significance = ns, $p < 0.05$*, $p < 0.01$**, $p < 0.001$***, $p < 0.0001$****. One-way ANOVA was performed in (C), (G), (H), (I), and (J) as discovery test. Unpaired two-tailed t tests were performed as post hoc tests.

See also Figure S5.

interaction might also be operational in stem-like AML cells (Figures 7D–7F and S5I).

Interestingly, human AMLs with genomic alterations capable of transforming only HSCs, such as *FLT3*-ITD AMLs (without *NPM1* alterations), displayed a transcriptomic state of stemness and expressed consistently high levels of the MHC-II machinery (Figure 7G). In contrast, AMLs with *NPM1* mutations (without *FLT3* alterations), capable of also transforming differentiated

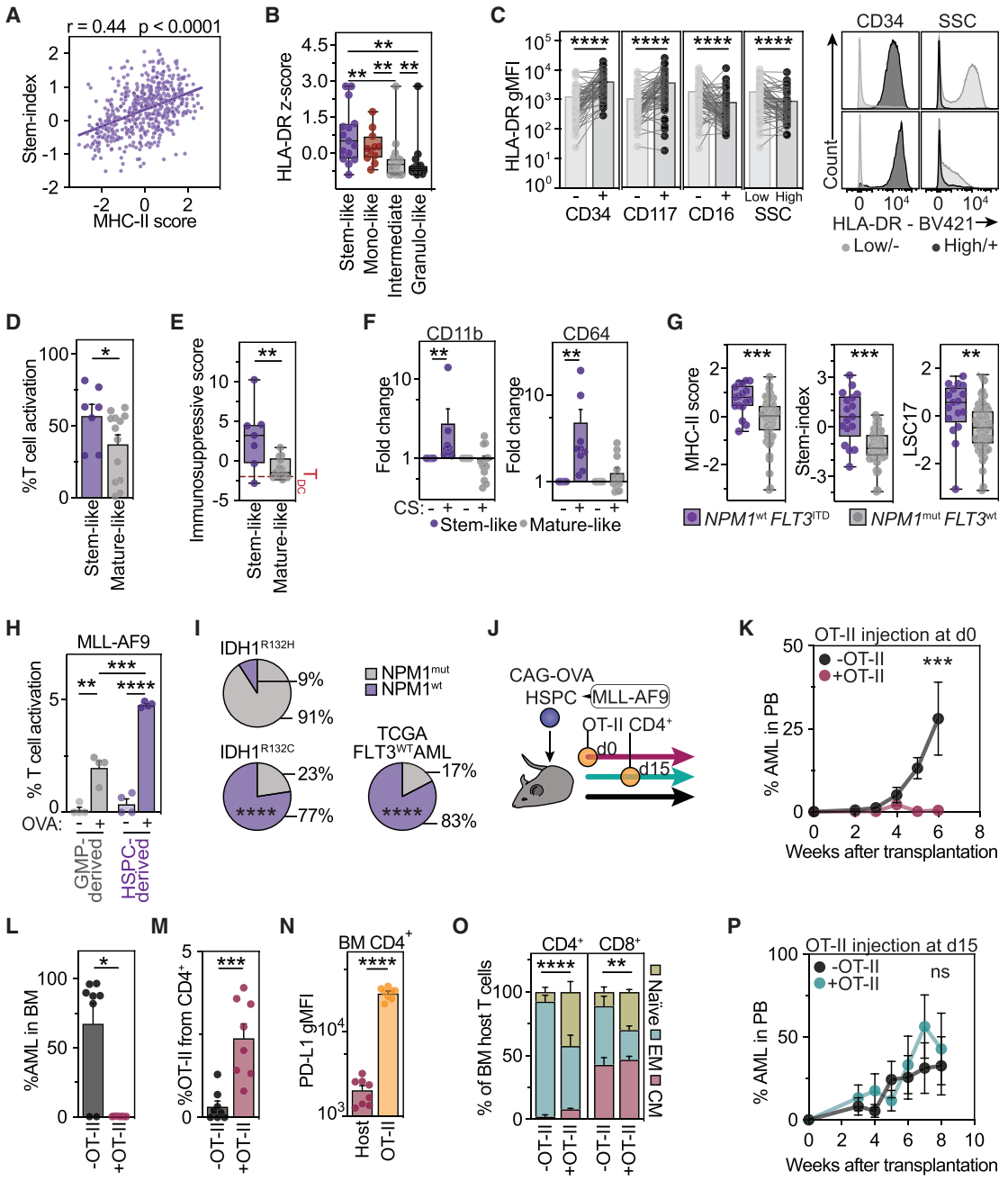

Figure 7. MHC-II-mediated neoantigen presentation of HSPCs protects from leukemia onset

(A) Stemness correlates with MHC-II expression in AML. Sum of scaled HLA-DR (MHC-II) gene expression and stem cell scores for AMLs from Pölönen et al. (2019), n = 523.

(B and C) AML patient samples were analyzed by flow cytometry and stratified into indicated groups.

(B) HLA-DR surface expression in the different AML groups, n = 63.

(C) HLA-DR geometric mean fluorescence intensity within AML blasts positive or negative for representative stem or mature markers (left), n = 63. Representative flow cytometry histograms (right).

(D) T cell activation capability in AML cell lines stratified as stem-like or mature-like, n = 23.

(E) Immunosuppressive score in activated $CD4^+$ T cells in the presence of the AML cell lines from D based on the *Z* scored expression of LAG3, PD-L1, and TIM3, n = 23.

(F) CD11b (left) and CD64 (right) expression in AML cell lines after coculture with $CD4^+$ T cell in the presence or absence of CS, n = 23.

(G) Sum of scaled MHC-II related genes (left) or stem cell scores (Ng et al., 2016) (right) in AML patients segregated based on NPM1 and FLT3 mutational state (Kohlmann et al., 2010), n = 78.

(H) Antigen presentation assays of HSC- and GMP-derived MLL-AF9 leukemias, n = 4.

(legend continued on next page)

progenitors, displayed a more differentiated phenotype and lower expression of the MHC-II machinery. These data suggest that the leukemic cell origin might determine the APC capacity of the AML. To experimentally test this, we generated stem cell-derived AMLs and mature granulocyte progenitor-derived AMLs by transducing either mouse LSK or GMP populations with the oncogene *MLL-AF9*, followed by transplantation into recipient mice (Krivtsov et al., 2006, 2013). In line with our hypothesis, stem cell-derived AMLs expressed more MHC-II and were significantly more efficient in inducing MHC-II-dependent, antigen-specific $CD4^+$ T cell responses, if compared with myeloid progenitor-derived AMLs (Figures 7H, S5J, and S5K). Together, these data demonstrate that the state of differentiation, linked to the cellular origin of AML, impacts on the capability of the disease to interact with the adaptive immune system. Moreover, similar to their healthy counterparts, stem cell-like leukemia cells display most efficient APC function, which is lost during granulocytic differentiation.

MHC-II-mediated interactions between transformed stem cells and antigen-specific $CD4^+$ T cells prevent leukemia onset

Since healthy and malignant stem cells displayed APC capacities, we investigated whether the above-described mechanism driving differentiation and depletion of immunogenic antigen-presenting stem cells could serve as an immunosurveillance mechanism to prevent leukemia onset by eliminating transformed HSPCs. According to our hypothesis, mutations generating MHC-II restricted neoantigens in humans should be efficiently out-selected in stem-like AMLs, but not in differentiated leukemias that express low levels of MHC-II, such as $NPM1^{mut}$ AMLs. In line with this, the IDH1(R132H) mutation, generating a well-established MHC-II-restricted neoepitope (Schumacher et al., 2014), occurred almost exclusively in differentiated $NPM1^{mut}$ AML but not in more immature $NPM1^{wt}$ AMLs (Figure 7I). In contrast, AMLs with a nonimmunogenic IDH1(R132C) mutation displayed a comparable proportion of $NPM1^{mut}$ AMLs with a general AML cohort, supporting the hypothesis that immature HSPCs acquiring immunogenic aberrations presented via MHC-II are efficiently removed from the hematopoietic system in humans.

To experimentally validate this hypothesis, we mimicked a malignant transformation resulting in immunogenic neoantigen presentation by transforming OVA-expressing HSPCs with the oncogene *MLL-AF9*, followed by transplantation into mice in the presence or absence of OVA-specific OT-II $CD4^+$ T cells (Figure 7J). While mice rapidly developed leukemias in the absence of $CD4^+$ T cells that specifically recognize the malignant leukemia stem cells, in the presence of OT-II T cells, transformed HSPCs were efficiently removed, preventing leukemia formation and accumulation of leukemia cells in the BM (Figures 7K and 7L). Similar to our observations in the healthy system, upon bidirectional interactions with leukemia stem cells *in vivo*, antigen-specific $CD4^+$ T cells expanded in the BM and acquired a PD-L1 high phenotype resembling T_{HSCs} capable of preventing harmful proinflammatory BM reactions (Figures 7M and 7N). In line with this, bystander BM T cells remained in a homeostatic state in the presence of PD-L1 high antigen-specific $CD4^+$ T cells but were highly activated in the absence of antigen-specific $CD4^+$ T cells (Figure 7O). Of note, although newly transformed stem cells were efficiently eliminated by interactions with $CD4^+$ T cells before disease onset, addition of antigen-specific $CD4^+$ T cells after the establishment of the disease did not rescue the animals (Figure 7P; see discussion). Together, these data suggest that presentation of immunogenic antigens by transformed stem cells act as surveillance mechanism to remove malignant cells from the hematopoietic system, thereby preventing leukemia onset.

DISCUSSION

Here, we demonstrate that mouse and human HSPCs present antigens via MHC-II and induce T cell responses. Interestingly, helper T cells have been described to regulate tissue homeostasis and stem cells in different tissues (Fujisaki et al., 2011; Burzyn et al., 2013; Arpaia et al., 2015; Ali et al., 2017; Biton et al., 2018; Hirata et al., 2018; Naik et al., 2018). In the intestine, MHC-II has been suggested to act as a scaffold for the recruitment of T helper subsets that modulate stem cell differentiation and tumorigenesis (Biton et al., 2018; Beyaz et al., 2021).

The acquisition of genomic aberrations in HSPCs is the main cause for the development of hematological malignancies. Accordingly, several passive protection mechanisms reduce the exposure of HSPCs to molecular, cellular, and inflammatory stress, minimizing the risk for a malignant transformation (Essers et al., 2009; Sato et al., 2009; Fujisaki et al., 2011; van Galen

(I) Proportion of $NPM1^{wt}$ or $NPM1^{mut}$ co-occurrence with immunogenic $IDH1^{R132H}$ (n = 33), non-immunogenic $IDH1^{R132C}$ (n = 31) and $FLT3^{wt}$ AMLs (n = 144) (Ley et al., 2013; Falini et al., 2019).
(J–P) Stem cell-derived leukemia antigen presentation impacts on disease onset.
(J) Experimental scheme. CAG-OVA HSPCs were transformed with MLL-AF9 and cotransplanted with or without OT-II T cells at day 0 (K-O) or 2 weeks post-transplantation (P).
(K and P) AML cells over time in the peripheral blood, n = 5–8.
(L) AML cells in the BM at the endpoint, n = 8.
(M) OT-II $CD4^+$ T cells in the BM at the endpoint, n = 8.
(N) PD-L1 expression in BM $CD4^+$ T cells, n = 8.
(O) Relative frequencies of host $CD4^+$ (left) and $CD8^+$ (right) naive, effector memory (EM) and central memory (CM) T cells in presence or absence of OT-II $CD4^+$ T cells, n = 8.
Individual values are shown in (A). Minimum to maximum are depicted in (E) and (G), means and SEM are depicted otherwise. No significance = ns, $p < 0.05$*, $p < 0.01$**, $p < 0.001$***, $p < 0.0001$****. Two-way ANOVA (H) or Kruskal-Wallis (B and F) were performed as discovery tests. Linear regression analysis (A), chi-squared test (I), two-way ANOVA (K, O, and P), paired (C and F) unpaired Mann-Whitney test (B, D, E, G, and L) was performed. If not stated otherwise, unpaired two-tailed t tests were performed as post hoc tests.
See also Figure S5.

et al., 2014; Walter et al., 2015; Zhang et al., 2016; Ho et al., 2017). In addition, Tregs have been implicated in maintaining HSC quiescence and establishing an immune privileged niche to further protect HSPC integrity (Zou et al., 2004; Urbieta et al., 2010; Fujisaki et al., 2011; Pierini et al., 2017; Hirata et al., 2018). However, active mechanisms that specifically eliminate aberrant HSPCs from the stem cell pool have not been described to date. Here, we demonstrate that mouse and human HSPCs continuously present antigens via MHC-II and use this process as an immunosurveillance mechanism. Although the presentation of self-antigens during homeostasis is immunologically ignored, the presentation of immunogenic antigens results in a bidirectional interaction between antigen-presenting HSPCs and antigen-specific $CD4^+$ T cells. Within the HSPC pool, antigen-specific interactions with $CD4^+$ T cells trigger a rapid cycle entry and differentiation specifically of those HSPCs that present immunogenic antigens, thereby effectively eliminating potentially (pre)malignant HSPCs. Simultaneously, this bidirectional interaction results in the activation $CD4^+$ T cells. However, in contrast to proinflammatory antigen-specific interactions, $CD4^+$ T cells are polarized to an immunoregulatory state, thereby preventing excessive inflammatory responses in the BM that would endanger the remaining healthy HSPCs (Sato et al., 2009; Walter et al., 2015).

In our study, we have investigated the effect of the presentation of immunogenic antigens derived from endogenous sources on HSPCs, reflecting the presentation of neoantigens during leukemogenesis, which trigger the effective elimination of (pre)malignant HSPCs. However, similar safeguarding mechanisms might be in place, in which the presentation of exogenous pathogen-derived peptides could drive the rapid elimination of infected HSPCs.

All in all, our data demonstrate that MHC-II based antigen presentation by HSPCs acts an immunosurveillance mechanism operational both in mouse and in human, providing a mechanistic understanding for the recent clinical findings that relapse after allogeneic stem cell transplantation is tightly associated with the loss of MHC-II in AML (Christopher et al., 2018; Toffalori et al., 2019). These findings may also provide a potential explanation for the heterogeneous response of AMLs to immunotherapies (Liao et al., 2019; Barrett, 2020; Vago and Gojo, 2020). Boosting or restoring MHC-II-mediated antigen presentation might serve as a future therapeutic avenue to prevent AML relapse. Lastly, a deregulation of this immunoregulatory MHC-II-T cell axis might also result in loss of stem cell function as observed in acquired idiopathic aplastic anemia, an autoimmune disease caused by the immune-mediated destruction of HSCs. In this line, particular MHC-II haplotypes and loss of heterozygosity are associated with aplastic anemia susceptibility and response to immunosuppressive therapy (Nakao et al., 1994; Nimer et al., 1994; Sauntharajah et al., 2002; Rehman et al., 2009; Dhaliwal et al., 2011; Liu et al., 2016; Young, 2018).

Together, our study reveals so far unrecognized insights into antigen-specific bidirectional interactions between HSPCs and $CD4^+$ T cells, demonstrating that HSPCs are not only passive receivers of immunological signals but also actively engage in adaptive immune responses to safeguard the integrity of the stem cell pool.

Limitations of the study

Our study has uncovered a novel immunosurveillance that is driven by a direct, MHC-II-dependent interaction between antigen-specific $CD4^+$ T cells and antigen-presenting HSPCs. Although there is no evidence for a direct participation of $CD8^+$ T cells in the elimination of malignant HSPCs, we cannot completely rule out that secondary activation of $CD8^+$ T cells may play a role in some experimental settings. Although our data demonstrate that leukemic HSPCs are rapidly cleared upon presentation of immunogenic neoantigens via MHC-II during disease onset, the functional role of MHC-II in fully established leukemias remains more elusive. Since antigen presentation by HSPCs polarizes $CD4^+$ T cells to an immunoregulatory state, it is conceivable that fully established leukemias may hijack this mechanism to create an immune suppressive environment and evade immune clearance. In line with this, immune suppression is frequently observed in AML (Vago and Gojo, 2020).

STAR★METHODS

Detailed methods are provided in the online version of this paper and include the following:

- KEY RESOURCES TABLE
- RESOURCE AVAILABILITY
  - Lead contact
  - Materials availability
  - Data and code availability
- EXPERIMENTAL MODEL AND SUBJECT DETAILS
  - Mice
  - Human samples
- METHOD DETAILS
  - Preparation of mouse bone marrow, spleen and lymph nodes
  - Flow cytometry staining, acquisition and FACS sorting
  - Quantitative Polymerase Chain Reaction (qPCR)
  - Murine *ex vivo* cultures
  - Human *ex vivo* cultures
  - BM transplantation
  - Adoptive co-transfer of OVA-loaded HSCs and antigen-specific T cells
  - *In vivo* antigen presentation assays
  - MLL-AF9 experiments
  - Immunopeptidomics
  - NanoString and RNA-Seq gene expression analysis
  - *In vitro* suppression assay
  - *In vitro* $CD8^+$ T cell cytotoxicity assay
  - *In vitro* macrophage polarization assay
  - *In vivo* suppression assay
  - EuroFlow analysis of diagnostic AML samples
  - Quantification and statistical analysis

SUPPLEMENTAL INFORMATION

Supplemental information can be found online at https://doi.org/10.1016/j.stem.2022.04.007.

ACKNOWLEDGMENTS

We would like to thank all members from the DKFZ flow cytometry, the DKFZ animal facility, D. Kozoriz, and J. Panten for their assistance. We thank L. Bunse and M. Platten for providing the MHC-II conditional knockout mouse

model. This work was supported by a German Academic Scholarship Foundation PhD fellowship (to A.S.); the Emmy Noether fellowship RA3166/1-1 funded by the Deutsche Forschungsgemeinschaft (DFG) (to S. Raffel); the P01AI073748 and R01NS030843 funded by the National Institute of Health (NIH) (to V.K.K.); the SFB873 (to A.T.), FOR2674 (to A.T. and L.B.), and FOR2033 (to A.T.) funded by the DFG; the SyTASC consortium (Deutsche Krebshilfe) (all to A.T. and L.B.); the Dietmar Hopp Foundation and the José Carreras Foundation for Leukemia Research (grant no. DCJLS 20R/2017) (both to A.T. and S.H.); and the LeukoSyStem consortium (BMBF) (to S. Raffel and S.H.).

AUTHOR CONTRIBUTIONS

Conceptualization, S.H. and P.H.-M.; methodology, P.H.-M., D.V., and A.S.; investigation, P.H.-M., D.V., A.S., H.J.U., M.G., A.B., M.A.A.M., S.-L.L., E.v.d.S., C.L.T., C.H., P.S.W., D.E., K.O.D., N.C., E.D., F.P., A.P., and C.K.; formal analysis, P.H.-M., F.G., C.R., and C.A.; resources, S. Renders, C.R., S. Raffel, R.L., T.B., W.O., M.D.M., M.A.G.E., S.B.E., W.-K.H., D.N., M.H., C.T., L.B., C.M.-T., and D.H.; writing – original draft, S.H. and P.H.-M.; writing – review & editing, S.H., P.H.-M., and D.V.; funding acquisition, S.H., A.T., and V.K.K.; supervision, S.H., A.T., and V.K.K.

DECLARATION OF INTERESTS

V.K.K. is a cofounder, has ownership interest, and is on the SAB of Celsius Therapeutics and Tizona Therapeutics.

Received: June 29, 2020
Revised: December 8, 2021
Accepted: April 8, 2022
Published: May 5, 2022

SUPPORTING CITATIONS

The following references appear in the supplemental information: Alshetaiwi et al., 2020.

REFERENCES

Ali, N., Zirak, B., Rodriguez, R.S., Pauli, M.L., Truong, H.A., Lai, K., Ahn, R., Corbin, K., Lowe, M.M., Scharschmidt, T.C., et al. (2017). Regulatory T cells in skin facilitate epithelial stem cell differentiation. Cell *169*, 1119–1129.

Alshetaiwi, H., Pervolarakis, N., McIntyre, L.L., Ma, D., Nguyen, Q., Rath, J.A., Nee, K., Hernandez, G., Evans, K., Torosian, L., et al. (2020). Defining the emergence of myeloid-derived suppressor cells in breast cancer using single-cell transcriptomics. Sci. Immunol. *5*, eaay6017.

Arpaia, N., Green, J.A., Moltedo, B., Arvey, A., Hemmers, S., Yuan, S., Treuting, P.M., and Rudensky, A.Y. (2015). A distinct function of regulatory T cells in tissue protection. Cell *162*, 1078–1089.

Baldridge, M.T., King, K.Y., Boles, N.C., Weksberg, D.C., and Goodell, M.A. (2010). Quiescent haematopoietic stem cells are activated by IFN-γ in response to chronic infection. Nature *465*, 793–797.

Barnden, M.J., Allison, J., Heath, W.R., and Carbone, F.R. (1998). Defective TCR expression in transgenic mice constructed using cDNA-based α- and β-chain genes under the control of heterologous regulatory elements. Immunol. Cell Biol. *76*, 34–40.

Barrett, A.J. (2020). Acute myeloid leukaemia and the immune system: implications for immunotherapy. Br. J. Haematol. *188*, 147–158.

Berlin, C., Kowalewski, D.J., Schuster, H., Mirza, N., Walz, S., Handel, M., Schmid-Horch, B., Salih, H.R., Kanz, L., Rammensee, H., et al. (2015). Mapping the HLA ligandome landscape of acute myeloid leukemia: a targeted approach toward peptide-based immunotherapy. Leukemia *29*, 647–659.

Bettelli, E., Pagany, M., Weiner, H.L., Linington, C., Sobel, R.A., and Kuchroo, V.K. (2003). Myelin oligodendrocyte glycoprotein–specific T cell receptor transgenic mice develop spontaneous autoimmune optic neuritis. J. Exp. Med. *197*, 1073–1081.

Beyaz, S., Chung, C., Mou, H., Bauer-Rowe, K.E., Xifaras, M.E., Ergin, I., Dohnalova, L., Biton, M., Shekhar, K., Eskiocak, O., et al. (2021). Dietary suppression of MHC class II expression in intestinal epithelial cells enhances intestinal tumorigenesis. Cell Stem Cell *28*, 1922–1935.e5.

Biton, M., Haber, A.L., Rogel, N., Burgin, G., Beyaz, S., Schnell, A., Ashenberg, O., Su, C.W., Smillie, C., Shekhar, K., et al. (2018). T helper cell cytokines modulate intestinal stem cell renewal and differentiation. Cell *175*, 1307–1320.e22.

Burzyn, D., Kuswanto, W., Kolodin, D., Shadrach, J.L., Cerletti, M., Jang, Y., Sefik, E., Tan, T.G., Wagers, A.J., Benoist, C., et al. (2013). A special population of regulatory T cells potentiates muscle repair. Cell *155*, 1282–1295.

Cabezas-Wallscheid, N., Klimmeck, D., Hansson, J., Lipka, D.B., Reyes, A., Wang, Q., Weichenhan, D., Lier, A., von Paleske, L., Renders, S., et al. (2014). Identification of regulatory networks in HSCs and their immediate progeny via integrated proteome, transcriptome, and DNA methylome analysis. Cell Stem Cell *15*, 507–522.

Charrad, M., Ghazzali, N., Boiteau, V., and Niknafs, A. (2014). Nbclust: an R package for determining the relevant number of clusters in a data set. J. Stat. Software *61*, 1–36.

Chihara, N., Madi, A., Kondo, T., Zhang, H., Acharya, N., Singer, M., Nyman, J., Marjanovic, N.D., Kowalczyk, M.S., Wang, C., et al. (2018). Induction and transcriptional regulation of the co-inhibitory gene module in T cells. Nature *558*, 454–459.

Christopher, M.J., Petti, A.A., Rettig, M.P., Miller, C.A., Chendamarai, E., Duncavage, E.J., Klco, J.M., Helton, N.M., O'Laughlin, M., Fronick, C.C., et al. (2018). Immune escape of relapsed AML cells after allogeneic transplantation. N. Engl. J. Med. *379*, 2330–2341.

Collison, L.W., Chaturvedi, V., Henderson, A.L., Giacomin, P.R., Guy, C., Bankoti, J., Finkelstein, D., Forbes, K., Workman, C.J., Brown, S.A., et al. (2010). IL-35-mediated induction of a potent regulatory T cell population. Nat. Immunol. *11*, 1093–1101.

Collison, L.W., Workman, C.J., Kuo, T.T., Boyd, K., Wang, Y., Vignali, K.M., Cross, R., Sehy, D., Blumberg, R.S., and Vignali, D.A. (2007). The inhibitory cytokine IL-35 contributes to regulatory T-cell function. Nature *450*, 566–569.

Costello, R., Mallet, F., Chambost, H., Sainty, D., Arnoulet, C., Gastaut, J.A., and Olive, D. (1999). The immunophenotype of minimally differentiated acute myeloid leukemia (AML-M0): reduced immunogenicity and high frequency of CD34+/CD38− leukemic progenitors. Leukemia *13*, 1513–1518.

Dhaliwal, J.S., Wong, L., Kamaluddin, M.A., Yin, L.Y., and Murad, S. (2011). Susceptibility to aplastic anemia is associated with HLA-DRB1*1501 in an aboriginal population in Sabah, Malaysia. Hum. Immunol. *72*, 889–892.

Doulatov, S., Notta, F., Laurenti, E., and Dick, J.E. (2012). Hematopoiesis: a human perspective. Cell Stem Cell *10*, 120–136.

Durbin, J.E., Hackenmiller, R., Simon, M.C., and Levy, D.E. (1996). Targeted disruption of the mouse Stat1 gene results in compromised innate immunity to viral disease. Cell *84*, 443–450.

Eaves, C.J. (2015). Hematopoietic stem cells: concepts, definitions, and the new reality. Blood *125*, 2605–2613.

Essers, M.A.G., Offner, S., Blanco-Bose, W.E., Waibler, Z., Kalinke, U., Duchosal, M.A., and Trumpp, A. (2009). IFNα activates dormant haematopoietic stem cells in vivo. Nature *458*, 904–908.

Falini, B., Spinelli, O., Meggendorfer, M., Martelli, M.P., Bigerna, B., Ascani, S., Stein, H., Rambaldi, A., and Haferlach, T. (2019). IDH1-R132 changes vary according to NPM1 and other mutations status in AML. Leukemia *33*, 1043–1047.

Falk, K., Rötzschke, O., Stevanović, S., Jung, G., and Rammensee, H.G. (1991). Allele-specific motifs revealed by sequencing of self-peptides eluted from MHC molecules. Nature *351*, 290–296.

Fitchen, J.H., Foon, K.A., and Cline, M.J. (1981). The antigenic characteristics of hematopoietic stem cells. N. Engl. J. Med. *305*, 17–25.

Fujisaki, J., Wu, J., Carlson, A.L., Silberstein, L., Putheti, P., Larocca, R., Gao, W., Saito, T.I., Lo Celso, C., Tsuyuzaki, H., et al. (2011). In vivo imaging of T reg cells providing immune privilege to the haematopoietic stem-cell niche. Nature *474*, 216–219.

Genovese, G., Kähler, A.K., Handsaker, R.E., Lindberg, J., Rose, S.A., Bakhoum, S.F., Chambert, K., Mick, E., Neale, B.M., Fromer, M., et al. (2014). Clonal hematopoiesis and blood-cancer risk inferred from blood DNA sequence. N. Engl. J. Med. *371*, 2477–2487.

Goodnow, C.C., Sprent, J., Fazekas de St Groth, B., and Vinuesa, C.G. (2005). Cellular and genetic mechanisms of self tolerance and autoimmunity. Nature *435*, 590–597.

Gu, Z., Eils, R., and Schlesner, M. (2016). Complex heatmaps reveal patterns and correlations in multidimensional genomic data. Bioinformatics *32*, 2847–2849.

Haas, S., Hansson, J., Klimmeck, D., Loeffler, D., Velten, L., Uckelmann, H., Wurzer, S., Prendergast, Á.M., Schnell, A., Hexel, K., et al. (2015). Inflammation-induced emergency megakaryopoiesis driven by hematopoietic stem cell-like megakaryocyte progenitors. Cell Stem Cell *17*, 422–434.

Hay, S.B., Ferchen, K., Chetal, K., Grimes, H.L., and Salomonis, N. (2018). The Human Cell Atlas bone marrow single-cell interactive web portal. Exp. Hematol. *68*, 51–61.

Henri, S., Poulin, L.F., Tamoutounour, S., Ardouin, L., Guilliams, M., de Bovis, B., Devilard, E., Viret, C., Azukizawa, H., Kissenpfennig, A., et al. (2010). CD207+ CD103+ dermal dendritic cells cross-present keratinocyte-derived antigens irrespective of the presence of Langerhans cells. J. Exp. Med. *207*, 189–206.

Hirata, Y., Furuhashi, K., Ishii, H., Li, H.W., Pinho, S., Ding, L., Robson, S.C., Frenette, P.S., and Fujisaki, J. (2018). CD150high Bone Marrow Tregs Maintain Hematopoietic Stem Cell Quiescence and Immune Privilege via Adenosine. Cell Stem Cell *22*, 445–453.e5.

Hirche, C., Frenz, T., Haas, S.F., Döring, M., Borst, K., Tegtmeyer, P.K., Brizic, I., Jordan, S., Keyser, K., Chhatbar, C., et al. (2017). Systemic virus infections differentially modulate cell cycle state and functionality of long-term hematopoietic stem cells in vivo. Cell Rep. *19*, 2345–2356.

Ho, T.T., Warr, M.R., Adelman, E.R., Lansinger, O.M., Flach, J., Verovskaya, E.V., Figueroa, M.E., and Passegué, E. (2017). Autophagy maintains the metabolism and function of young and old stem cells. Nature *543*, 205–210.

Jaiswal, S., Fontanillas, P., Flannick, J., Manning, A., Grauman, P.V., Mar, B.G., Lindsley, R.C., Mermel, C.H., Burtt, N., Chavez, A., et al. (2014). Age-related clonal hematopoiesis associated with adverse outcomes. N. Engl. J. Med. *371*, 2488–2498.

Jakubzick, C.V., Randolph, G.J., and Henson, P.M. (2017). Monocyte differentiation and antigen-presenting functions. Nat. Rev. Immunol.) *17*, 349–362.

Jurewicz, M.M., and Stern, L.J. (2019). Class II MHC antigen processing in immune tolerance and inflammation. Immunogenetics *71*, 171–187.

Käll, L., Canterbury, J.D., Weston, J., Noble, W.S., and MacCoss, M.J. (2007). Semi-supervised learning for peptide identification from shotgun proteomics datasets. Nat. Methods *4*, 923–925.

Kambayashi, T., and Laufer, T.M. (2014). Atypical MHC class II-expressing antigen-presenting cells: can anything replace a dendritic cell? Nat. Rev. Immunol. *14*, 719–730.

Klimmeck, D., Cabezas-Wallscheid, N., Reyes, A., von Paleske, L., Renders, S., Hansson, J., Krijgsveld, J., Huber, W., and Trumpp, A. (2014). Transcriptome-wide profiling and posttranscriptional analysis of hematopoietic stem/progenitor cell differentiation toward myeloid commitment. Stem Cell Rep. *3*, 858–875.

Kohlmann, A., Bullinger, L., Thiede, C., Schaich, M., Schnittger, S., Döhner, K., Dugas, M., Klein, H.U., Döhner, H., Ehninger, G., et al. (2010). Gene expression profiling in AML with normal karyotype can predict mutations for molecular markers and allows novel insights into perturbed biological pathways. Leukemia *24*, 1216–1220.

Kowalewski, D.J., and Stevanović, S. (2013). Biochemical large-scale identification of MHC Class I ligands. Methods Mol. Biol. *960*, 145–157.

Krivtsov, A.V., Figueroa, M.E., Sinha, A.U., Stubbs, M.C., Feng, Z., Valk, P.J., Delwel, R., Döhner, K., Bullinger, L., Kung, A.L., et al. (2013). Cell of origin determines clinically relevant subtypes of MLL-rearranged AML. Leukemia *27*, 852–860.

Krivtsov, A.V., Twomey, D., Feng, Z., Stubbs, M.C., Wang, Y., Faber, J., Levine, J.E., Wang, J., Hahn, W.C., Gilliland, D.G., et al. (2006). Transformation from committed progenitor to leukaemia stem cell initiated by MLL-AF9. Nature *442*, 818–822.

Lê, S., Josse, J., and Husson, F. (2008). FactoMineR: an R package for multivariate analysis. J. Stat. Softw. *25*, 1–18.

Ley, T.J., Miller, C., Ding, L., Raphael, B.J., Mungall, A.J., Robertson, A., Hoadley, K., Triche, T.J., Laird, P.W., et al. (2013). Genomic and epigenomic landscapes of adult *de novo* acute myeloid leukemia. N. Engl. J. Med. *368*, 2059–2074.

Liao, D., Wang, M., Liao, Y., Li, J., and Niu, T. (2019). A review of efficacy and safety of checkpoint inhibitor for the treatment of acute myeloid leukemia. Front. Pharmacol. *10*, 609.

Liu, S., Li, Q., Zhang, Y., Li, Q., Ye, B., Wu, D., Wu, L., Lu, H., and Ji, C. (2016). Association of human leukocyte antigen DRB1*15 and DRB1*15:01 polymorphisms with response to immunosuppressive therapy in patients with aplastic anemia: a meta-analysis. PLoS One *11*, e0162382.

Love, M.I., Huber, W., and Anders, S. (2014). Moderated estimation of fold change and dispersion for RNA-seq data with DESeq2. Genome Biol. *15*, 550.

Maechler, M., Rousseeuw, P., Struyf, A., Hubert, M., and Hornik, K. (2019). Cluster: cluster analysis basics and extensions. R package version 2.1.0. https://CRAN.R-project.org/package=cluster.

Merad, M., Sathe, P., Helft, J., Miller, J., and Mortha, A. (2013). The dendritic cell lineage: ontogeny and function of dendritic cells and their subsets in the steady state and the inflamed setting. Annu. Rev. Immunol. *31*, 563–604.

Miale, T.D., Stenke, L.A., Lindblom, J.B., Sjögren, A.M., Reizenstein, P.G., Udén, A.M., and Lawson, D.L. (1982). Surface Ia-like expression and MLR-stimulating capacity of human leukemic myeloblasts: implications for immunotherapy and prognosis. Acta Haematol. *68*, 3–13.

Murphy, D.B., Lo, D., Rath, S., Brinster, R.L., Flavell, R.A., Slanetz, A., and Janeway, C.A. (1989). A novel MHC class II epitope expressed in thymic medulla but not cortex. Nature *338*, 765–768.

Mutis, T., Schrama, E., Melief, C.J., and Goulmy, E. (1998). CD80-transfected acute myeloid leukemia cells induce primary allogeneic T-cell responses directed at patient specific minor histocompatibility antigens and leukemia-associated antigens. Blood *92*, 1677–1684.

Mutis, T., Schrama, E., van Luxemburg-Heijs, S.A., Falkenburg, J.H., Melief, C.J., and Goulmy, E. (1997). HLA Class II restricted T-cell reactivity to a developmentally regulated antigen shared by leukemic cells and CD34+ early progenitor cells. Blood *90*, 1083–1090.

Naik, S., Larsen, S.B., Cowley, C.J., and Fuchs, E. (2018). Two to tango: dialog between immunity and stem cells in health and disease. Cell *175*, 908–920.

Nakao, S., Takamatsu, H., Chuhjo, T., Ueda, M., Shiobara, S., Matsuda, T., Kaneshige, T., and Mizoguchi, H. (1994). Identification of a specific HLA class II haplotype strongly associated with susceptibility to cyclosporine-dependent aplastic anemia. Blood *84*, 4257–4261.

Neefjes, J., Jongsma, M.L., Paul, P., and Bakke, O. (2011). Towards a systems understanding of MHC class I and MHC class II antigen presentation. Nat. Rev. Immunol. *11*, 823–836.

Ness, S., Lin, S., and Gordon, J.R. (2021). Regulatory dendritic cells, T cell tolerance, and dendritic cell therapy for immunologic disease. Front. Immunol. *12*, 633436.

Newman, R.A., Delia, D., Greaves, M.F., Navarrete, C., Fainboim, L., and Festenstein, H. (1983). Differential expression of HLA-DR and DR-linked determinants on human leukemias and lymphoid cells. Eur. J. Immunol. *13*, 172–176.

Ng, S.W.K., Mitchell, A., Kennedy, J.A., Chen, W.C., McLeod, J., Ibrahimova, N., Arruda, A., Popescu, A., Gupta, V., Schimmer, A.D., et al. (2016). A 17-gene stemness score for rapid determination of risk in acute leukaemia. Nature *540*, 433–437.

Nimer, S.D., Ireland, P., Meshkinpour, A., and Frane, M. (1994). An increased HLA DR2 frequency is seen in aplastic anemia patients. Blood *84*, 923–927.

Novershtern, N., Subramanian, A., Lawton, L.N., Mak, R.H., Haining, W.N., McConkey, M.E., Habib, N., Yosef, N., Chang, C.Y., Shay, T., et al. (2011).

Densely interconnected transcriptional circuits control cell states in human hematopoiesis. Cell *144*, 296–309.

Pellin, D., Loperfido, M., Baricordi, C., Wolock, S.L., Montepeloso, A., Weinberg, O.K., Biffi, A., Klein, A.M., and Biasco, L. (2019). A comprehensive single cell transcriptional landscape of human hematopoietic progenitors. Nat. Commun. *10*, 2395.

Picelli, S., Björklund, Å.K., Faridani, O.R., Sagasser, S., Winberg, G., and Sandberg, R. (2013). Smart-seq2 for sensitive full-length transcriptome profiling in single cells. Nat. Methods *10*, 1096–1098.

Picelli, S., Faridani, O.R., Björklund, A.K., Winberg, G., Sagasser, S., and Sandberg, R. (2014). Full-length RNA-seq from single cells using Smart-seq2. Nat. Protoc. *9*, 171–181.

Pierini, A., Nishikii, H., Baker, J., Kimura, T., Kwon, H.S., Pan, Y., Chen, Y., Alvarez, M., Strober, W., Velardi, A., et al. (2017). Foxp3+ regulatory T cells maintain the bone marrow microenvironment for B cell lymphopoiesis. Nat. Commun. *8*, 15068.

Pölönen, P., Mehtonen, J., Lin, J., Liuksiala, T., Häyrynen, S., Teppo, S., Mäkinen, A., Kumar, A., Malani, D., Pohjolainen, V., et al. (2019). Hemap: an interactive online resource for characterizing molecular phenotypes across hematologic malignancies. Cancer Res. *79*, 2466–2479.

Rehman, S., Saba, N., Khalilullah, Munir, S., Ahmed, P., and Mehmood, T. (2009). The frequency of HLA class I and II alleles in Pakistani patients with aplastic anemia. Immunol. Invest. *38*, 812–819.

Roche, P.A., and Furuta, K. (2015). The ins and outs of MHC class II-mediated antigen processing and presentation. Nat. Rev. Immunol. *15*, 203–216. 10.1038/nri3818.

Rudensky, A.Y., Rath, S., Preston-Hurlburt, P., Murphy, D.B., and Janeway, C.A. (1991). On the complexity of self. Nature *353*, 660–662.

Russell, J.L., and van den Engh, G.J. (1979). The expression of Histocompatibility-2 antigens on hemopoietic stem cells. Tissue Antigens *13*. 45–22.

Sato, T., Onai, N., Yoshihara, H., Arai, F., Suda, T., and Ohteki, T. (2009). Interferon regulatory factor-2 protects quiescent hematopoietic stem cells from type I interferon–dependent exhaustion. Nat. Med. *15*, 696–700.

Sauntharajah, Y., Nakamura, R., Nam, J.M., Robyn, J., Loberiza, F., Maciejewski, J.P., Simonis, T., Molldrem, J., Young, N.S., and Barrett, A.J. (2002). HLA-DR15 (DR2) is overrepresented in myelodysplastic syndrome and aplastic anemia and predicts a response to immunosuppression in myelodysplastic syndrome. Blood *100*, 1570–1574.

Schumacher, T., Bunse, L., Pusch, S., Sahm, F., Wiestler, B., Quandt, J., Menn, O., Osswald, M., Oezen, I., Ott, M., et al. (2014). A vaccine targeting mutant IDH1 induces antitumour immunity. Nature *512*, 324–327.

Sieff, C., Bicknell, D., Caine, G., Robinson, J., Lam, G., and Greaves, M.F. (1982). Changes in cell surface antigen expression during hemopoietic differentiation. Blood *60*, 703–713.

Spencer, S.D., Di Marco, F., Hooley, J., Pitts-Meek, S., Bauer, M., Ryan, A.M., Sordat, B., Gibbs, V.C., and Aguet, M. (1998). The orphan receptor CRF2-4 is an essential subunit of the interleukin 10 receptor. J. Exp. Med. *187*, 571–578.

Steimle, V., Otten, L.A., Zufferey, M., and Mach, B. (1993). Complementation cloning of an MHC class II transactivator mutated in hereditary MHC class II deficiency (or bare lymphocyte syndrome). Cell *75*, 135–146.

Steimle, V., Siegrist, C.A., Mottet, A., Lisowska-Grospierre, B., and Mach, B. (1994). Regulation of MHC class II expression by interferon-γ mediated by the transactivator gene CIITA. Science *265*, 106–109.

Steinman, R.M. (2007). Dendritic cells: understanding immunogenicity. Eur. J. Immunol. *37*, S53–S60.

Szer, J., Deeg, H.J., Appelbaum, F.R., and Storb, R. (1985). Failure of autologous marrow reconstitution after cytolytic treatment of marrow with anti-Ia monoclonal antibody. Blood *65*, 819–822.

Takizawa, H., Fritsch, K., Kovtonyuk, L.V., Saito, Y., Yakkala, C., Jacobs, K., Ahuja, A.K., Lopes, M., Hausmann, A., Hardt, W.D., et al. (2017). Pathogen-induced TLR4-TRIF innate immune signaling in hematopoietic stem cells promotes proliferation but reduces competitive fitness. Cell Stem Cell *21*, 225–240.e5.

Toffalori, C., Zito, L., Gambacorta, V., Riba, M., Oliveira, G., Bucci, G., Barcella, M., Spinelli, O., Greco, R., Crucitti, L., et al. (2019). Immune signature drives leukemia escape and relapse after hematopoietic cell transplantation. Nat. Med. *25*, 603–611.

Urbieta, M., Barao, I., Jones, M., Jurecic, R., Panoskaltsis-Mortari, A., Blazar, B.R., Murphy, W.J., and Levy, R.B. (2010). Hematopoietic progenitor cell regulation by CD4+CD25+ T cells. Blood *115*, 4934–4943.

Vago, L., and Gojo, I. (2020). Immune escape and immunotherapy of acute myeloid leukemia. J. Clin. Invest. *130*, 1552–1564.

van Dongen, J.J.M., Lhermitte, L., Böttcher, S., Almeida, J., van der Velden, V.H., Flores-Montero, J., Rawstron, A., Asnafi, V., Lécrevisse, Q., Lucio, P., et al. (2012). EuroFlow antibody panels for standardized n-dimensional flow cytometric immunophenotyping of normal, reactive and malignant leukocytes. Leukemia *26*, 1908–1975.

van Galen, P., Kreso, A., Mbong, N., Kent, D.G., Fitzmaurice, T., Chambers, J.E., Xie, S., Laurenti, E., Hermans, K., Eppert, K., et al. (2014). The unfolded protein response governs integrity of the haematopoietic stem-cell pool during stress. Nature *510*, 268–272.

Wakkach, A., Fournier, N., Brun, V., Breittmayer, J., Cottrez, F., and Groux, H. (2003). Characterization of dendritic cells that induce tolerance and T regulatory 1 cell differentiation in vivo. Immunity *18*, 605–617.

Walter, D., Lier, A., Geiselhart, A., Thalheimer, F.B., Huntscha, S., Sobotta, M.C., Moehrle, B., Brocks, D., Bayindir, I., Kaschutnig, P., et al. (2015). Exit from dormancy provokes DNA-damage-induced attrition in haematopoietic stem cells. Nature *520*, 549–552.

Young, N.S. (2018). Aplastic anemia. N. Engl. J. Med. *379*, 1643–1656.

Yu, G., Wang, L.G., Han, Y., and He, Q.Y. (2012). clusterProfiler: an R package for comparing biological themes Among gene clusters. OMICS A J. Integr. Biol. *16*, 284–287.

Zhang, H., Madi, A., Yosef, N., Chihara, N., Awasthi, A., Pot, C., Lambden, C., Srivastava, A., Burkett, P.R., Nyman, J., et al. (2020). An IL-27-driven transcriptional network identifies regulators of IL-10 expression across T Helper cell subsets. Cell Rep. *33*, 108433.

Zhang, H., Rodriguez, S., Wang, L., Wang, S., Serezani, H., Kapur, R., Cardoso, A.A., and Carlesso, N. (2016). Sepsis induces hematopoietic stem cell exhaustion and myelosuppression through distinct contributions of TRIF and MYD88. Stem Cell Rep. *6*, 940–956.

Zhu, J., and Paul, W.E. (2010). Peripheral CD4+ T-cell differentiation regulated by networks of cytokines and transcription factors. Immunol. Rev. *238*, 247–262.

Zou, L., Barnett, B., Safah, H., LaRussa, V.F., Evdemon-Hogan, M., Mottram, P., Wei, S., David, O., Curiel, T.J., and Zou, W. (2004). Bone marrow is a reservoir for CD4 + CD25 + Regulatory T cells that traffic through CXCL12/CXCR4 signals. Cancer Res. *64*, 8451–8455.

STAR★METHODS

KEY RESOURCES TABLE

REAGENT or RESOURCE	SOURCE	IDENTIFIER
Mouse antibodies		
Anti-mouse B220 FITC	ThermoFisher	RRID:AB_2621690
Anti-mouse B220 AF700	ThermoFisher	RRID: AB_891458
Anti-mouse B220 APC-efluor780	ThermoFisher	RRID:AB_2866434
Anti-mouse CD105 efluor 450	ThermoFisher	RRID:AB_10548959
Anti-mouse CD117 BV711	BioLegend	RRID:AB_2565956
Anti-mouse CD117 PE	ThermoFisher	RRID:AB_469643
Anti-mouse CD117 PE-Cy5	BioLegend	RRID:AB_468786
Anti-mouse CD11b FITC	ThermoFisher	RRID:AB_11152193
Anti-mouse CD11b AF700	ThermoFisher	RRID:AB_657586
Anti-mouse CD127 PE	BioLegend	RRID:AB_953562
Anti-mouse CD150 PE-Cy5	ThermoFisher	RRID:AB_493598
Anti-mouse CD16/32 AF700	ThermoFisher	RRID:AB_493995
Anti-mouse CD16/32 APC	ThermoFisher	RRID:AB_469356
Anti-mouse CD19 APC	BioLegend	RRID:AB_313646
Anti-mouse CD206 FITC	BioLegend	RRID:AB_10901166
Anti-mouse CD25 BV785	BioLegend	RRID:AB_2564131
Anti-mouse CD25 APC	BioLegend	RRID:AB_2280288
Anti-mouse CD274 (PD-L1) BV711	BioLegend	RRID:AB_2563619
Anti-mouse CD274 (PD-L1) PE	BioLegend	RRID:AB_2073556
Anti-mouse CD279 (PD-1) APC	ThermoFisher	RRID:AB_11149358
Anti-mouse CD34 PE	ThermoFisher	RRID:AB_467210
Anti-mouse CD3e FITC	ThermoFisher	RRID:AB_2572431
Anti-mouse CD3e	BioXCell	RRID:AB_1107632
Anti-mouse CD4 BUV805	BD	RRID:AB_2827960
Anti-mouse CD4 FITC	ThermoFisher	RRID:AB_464892
Anti-mouse CD4 AF700	ThermoFisher	RRID:AB_493999
Anti-mouse CD4 APC-Cy7	BD	RRID:AB_394331
Anti-mouse CD41 APC	BioLegend	RRID:AB_11126751
Anti-mouse CD41 FITC	BD	RRID:AB_10892804
Anti-mouse CD44 FITC	BioLegend	RRID:AB_312957
Anti-mouse CD45 Pacific Blue	BioLegend	RRID:AB_493536
Anti-mouse CD45.1 BUV395	BD	RRID:AB_2722493
Anti-mouse CD45.1 BV605	BioLegend	RRID:AB_11204076
Anti-mouse CD45.1 PE	ThermoFisher	RRID:AB_465675
Anti-mouse CD45.1 PE-Cy5	ThermoFisher	RRID:AB_468759
Anti-mouse CD45.2 FITC	ThermoFisher	RRID:AB_465061
Anti-mouse CD45.2 APC-efluor780	ThermoFisher	RRID:AB_1272211
Anti-mouse CD48 BUV395	BD	RRID:AB_2739984
Anti-mouse CD48 APC	ThermoFisher	RRID:AB_469408
Anti-mouse CD48 BV421	BioLegend	RRID:AB_10895922
Anti-mouse CD69 PE-Cy5	BioLegend	RRID:AB_313112
Anti-mouse CD8 BUV395	BD	RRID:AB_2739421
Anti-mouse CD8 FITC	ThermoFisher	RRID:AB_464915
Anti-mouse CD8 AF700	ThermoFisher	RRID:AB_494005

(*Continued on next page*)

Continued

REAGENT or RESOURCE	SOURCE	IDENTIFIER
Anti-mouse CD84 PE	BioLegend	RRID:AB_2074756
Anti-mouse CD90.1 FITC	BioLegend	RRID:AB_314014
Anti-mouse F4/80 Pacific Blue	ThermoFisher	RRID:AB_10373419
Anti-mouse Gr-1 FITC	ThermoFisher	RRID:AB_11152477
Anti-mouse Gr-1 AF700	ThermoFisher	RRID:AB_494007
Anti-mouse Ki67 PE-Cy7	BD	RRID:AB_10716060
Anti-mouse Lag3 APC-Cy7	ThermoFisher	RRID:AB_2637323
Anti-mouse MHC-II (I-A/I-E)	BioXCell	RRID:AB_10949298
Anti-mouse MHC-II (I-A/I-E) BV785	BioLegend	RRID:AB_2565977
Anti-mouse MHC-II (I-A/I-E) PE	BioLegend	RRID:AB_313323
Anti-mouse IL-10 PE	BioLegend	RRID:AB_466176
Anti-mouse Sca-1 APC-Cy7	BD	RRID:AB_1727552
Anti-mouse SiglecF BV421	BD	RRID:AB_2739398
Anti-mouse SiglecH PE	ThermoFisher	RRID:AB_10597139
Anti-mouse TCRb PE-Cy7	Biolegend	RRID:AB_893627
Anti-mouse Ter119 FITC	ThermoFisher	RRID:AB_465312
Anti-mouse Ter119 AF700	BioLegend	RRID:AB_528963
Anti-mouse Tim3 APC	BioLegend	Clone:5D12 (custom)
Anti-mouse I-Ab-Ea FITC	ThermoFisher	RRID:AB_996692
Anti-mouse I-Ab-Ea Biotin	ThermoFisher	RRID:AB_657823
Human antibodies		
Anti-human CD3 BUV395	BD	RRID:AB_2744387
Anti-human CD4 APC	BD	RRID:AB_11153855
Anti-human CD4 BUV805	ThermoFisher	RRID:AB_2870176
Anti-human CD8 APC	BD	RRID:AB_398595
Anti-human CD11b APC	BD	RRID:AB_10561676
Anti-human CD11c BV605	BD	RRID:AB_2744276
Anti-human CD11c Pe-Cy7	BioLegend	RRID:AB_389351
Anti-human CD19 APC	ThermoFisher	RRID:AB_10804519
Anti-human CD19 APC-Cy7	BioLegend	RRID:AB_2564193
Anti-human CD19 BV786	BioLegend	RRID:AB_2563442
Anti-human CD20 APC	BD	RRID:AB_398670
Anti-human CD25 PE-Cy7	BioLegend	RRID:AB_314282
Anti-human CD33 BV421	BioLegend	RRID:AB_2561690
Anti-human CD34 APC-Cy7	ThermoFisher	RRID:AB_2573956
Anti-human CD38 A700	ThermoFisher	RRID:AB_10852837
Anti-human CD41a APC	BioLegend	RRID:AB_2129464
Anti-human CD45 APC	ThermoFisher	RRID:AB_10667894
Anti-human CD45 PE	ThermoFisher	RRID:AB_1724079
Anti-human CD45RA FITC	BioLegend	RRID:AB_2650650
Anti-human CD45RO FITC	BioLegend	RRID:AB_2564159
Anti-human CD49b FITC	BioLegend	RRID:AB_2562531
Anti-human CD49f PE-Cy7	ThermoFisher	RRID:AB_10804881
Anti-human CD56 APC	BD	RRID:AB_398601
Anti-human CD56 Alexa Fluor 488	BD	RRID:AB_396808
Anti-human CD56 BV711	BioLegend	RRID:AB_2562417
Anti-human CD69 BUV395	BD	RRID:AB_2738770
Anti-human CD90 PE-Cy5	BD	RRID:AB_395971
Anti-human HLA-DR PE	ThermoFisher	RRID:AB_10698015

(*Continued on next page*)

Continued

REAGENT or RESOURCE	SOURCE	IDENTIFIER
Anti-human CD154 PE-Cy5	BioLegend	RRID:AB_314831
Anti-human CD197 (CCR7) Pacific Blue	BioLegend	RRID:AB_10918984
Anti-human CD223 (LAG3) BV711	BioLegend	RRID:AB_2716125
Anti-human CD235 APC	ThermoFisher	RRID:AB_2043823
Anti-human CD274 (PD-L1) BV785	BioLegend	RRID:AB_2629582
Anti-human CD279 (PD1) APC	BioLegend	RRID:AB_940473
Anti-human CD366 (TIM3) BV605	BioLegend	RRID:AB_2562194
Bacterial and virus strains		
MCMV-Δm157 (MCMV)	Hirche et al., 2017	N/A
Biological samples		
Human Healthy Bone Marrow Aspirates	Heidelberg University Hospital	N/A
Human Peripheral Blood	University Hospital Mannheim	N/A
Human AML Bone Marrow Aspirates	AML-SG and SAL biorepositories	N/A
Chemicals, peptides, and recombinant proteins		
pI:C	Invivogen	Cat#tlrl-pic
LPS	ThermoFisher	Cat#00-4976-03
IFNα	Miltenyi	Cat#130-093-131
Ovalbumin	Invivogen	Cat#vac-stova
DQ Ovalbumin	Invitrogen	Cat#D12053
Ovalbumin 323-339 peptide	Invivogen	Cat#vac-isq
Ovalbumin 257-264 peptide	Invivogen	Cat#vac-sin
MOG peptide	Genemed Sythesis	Cat#MOG3555-P2-1
Eα peptide (52-68)	Mimotopes	Cat#68827-005
ACK Buffer	Lonza	Cat#10-548E
Sodium pyruvate	Gibco	Cat#11360039
L-Glutamine	Gibco	Cat#25030081
L-arginine	Sigma	Cat#A5006-100G
L-asparagine	Sigma	Cat#A0884-100G
Penicillin/Streptomycin	Sigma	Cat#P4458-100ml
Folic acid	Sigma	Cat#F7876-10G
MEM non-essential amino acids	ThermoFisher	Cat#11140050
MEM vitamin solution	ThermoFisher	Cat#11120052
β-mercaptoethanol	Sigma	Cat# M3148
Cell Trace Violet	ThermoFisher	Cat#C34557
Dynabeads Mouse T-Activator	ThermoFisher	Cat#11452D
CytoStim	Miltenyi	Cat#130-092-172
PepMix CEFX Ultra SuperStim MHC-II Subset Pool	JPT	Cat#PM-CEFX-3
Mouse TPO	PreproTech	Cat#315-14
Mouse SCF	PreproTech	Cat#250-03
CNBr-activated Sepharose	GE Healthcare	Cat#17-0430-01
Trifluoroacetic acid	Merck	Cat#108262
DNAseI	Roche	Cat#4716728001
2′,7′-Dichlorofluorescin diacetate	Sigma	Cat#D6883-50MG
DAPI	ThermoFisher	RRID:AB_2629482
Sunflower oil	Sigma	S5007-250ML
Tamoxifen	Sigma	T5648-1G
RNAsin+	Promega	N2611
Triton X-100	Sigma	9002-93-1
Smart-seq2 Oligo-dT primer	Sigma	N/A

(*Continued on next page*)

Continued

REAGENT or RESOURCE	SOURCE	IDENTIFIER
dNTP mix	NEB	N0447S
SmartScribe	Takara	639538
Smart-seq2 TSO	IDT	N/A
Smart-seq2 ISPCR primer	IDT	N/A
Ctrl IgG2b	ThermoFisher	RRID:AB_470099
Streptavidin PE	BioLegend	Cat#12-4317-82
Critical commercial assays		
Dynabeads Untouched Mouse CD4 Cells Kit	Invitrogen	Cat#11416D
Cell Stimulation Cocktail (plus protein transport inhibitors)	eBioscience	Cat#00-4975-93
Fixation/Permeabilization Solution Kit	BD	Cat#554714
Arcturus PicoPure RNA Isolation Kit	Invitrogen	Cat#KIT0204
SuperScript VILO cDNA synthesis Kit	Invitrogen	Cat#11754050
PowerUP SybrGreen Mastermix	ThermoFisher	Cat#A25741
RNA 6000 Pico Kit	Agilent	Cat#5067-1513
SMARTer Ultra Low Input RNA Kit	Takara	Cat# 634940
NEBNext ChIP-seq Library Prep Kit for Illumina	NEB	Cat# E6240
Qubit™ dsDNA HS Assay Kit	Invitrogen	Cat# Q32851
SureSelect HS XT Target Enrichment System v6	Agilent	N/A
KAPA HiFi HS Mastermix	Roche	Cat#07958935001
Experimental models: Mice		
BALB/c	Harlan / Jackson / Taconic	JAX:000651
C57BL/6J	Harlan/Taconic/Jackson Laboratory	JAX:000664
B6.SJL-Ptprca Pepcb/BoyJ	Harlan/Taconic/Jackson Laboratory	JAX:002014
NOD.Cg-PrkdcscidIL2rgtmWjl/SzJ	Jackson	JAX:005557
C57BL/6-Tg(CAG-OVA)916Jen/J	Jackson	JAX:005145
C57BL/6-Tg(Tcra2D2,Tcrb2D2)1Kuch/J	Jackson	JAX:006912
B6.Cg-Tg(TcraTcrb)425Cbn/J	Jackson	JAX:004194
C57BL/6-Tg(TcraTcrb)1100Mjb/J	Jackson	JAX:003831
B6.129S2-Il10rbtm1Agt/J	Jackson	JAX:005027
B6.129S(Cg)-Stat1tm1Dlv/J	Durbin et al., 1996	JAX:012606
BALB/c x C57BL/6J	N/A	N/A
B6-Tg(Tal1-cre)42-056Jrg H2-Ab1tm1Koni Gt(ROSA)26Sortm1(EYFP)Cos/Atp	N/A	N/A
H2-Ab1tm1Koni Gt(ROSA)26Sortm1(EYFP)Cos/Atp	N/A	N/A
Experimental models: Cell lines		
CTV-1	Leibniz Institute DSMZ	ACC 40
GDM-1	Leibniz Institute DSMZ	ACC 87
HL-60	Cell Lines Service (CLS)	300209
Kasumi-1	Leibniz Institute DSMZ	ACC 220
Kasumi-3	Leibniz Institute DSMZ	16469
Kasumi-6	Leibniz Institute DSMZ	15974
KG-1	Leibniz Institute DSMZ	ACC 14
KG-1a	Leibniz Institute DSMZ	ACC 421
ME-1	Leibniz Institute DSMZ	ACC 537
ML-1	Leibniz Institute DSMZ	ACC 464
ML-2	Leibniz Institute DSMZ	ACC 15

(*Continued on next page*)

Continued

REAGENT or RESOURCE	SOURCE	IDENTIFIER
MOLM-14	Leibniz Institute DSMZ	ACC 777
MONO-MAC-6	Leibniz Institute DSMZ	ACC 124
MV4-11	American Type Culture Collection (ATCC)	ATCC-CRL-9591
NB-4	Leibniz Institute DSMZ	ACC 207
OCI-AML2	Leibniz Institute DSMZ	ACC 99
OCI-AML3	Leibniz Institute DSMZ	ACC 582
OCI-M1	Leibniz Institute DSMZ	ACC 529
PL-21	Leibniz Institute DSMZ	ACC 536
SET-2	Leibniz Institute DSMZ	ACC 608
SKM-1	Leibniz Institute DSMZ	ACC 547
THP-1	Leibniz Institute DSMZ	ACC 16
U-937	Leibniz Institute DSMZ	ACC 5
YNH-1	Leibniz Institute DSMZ	ACC 692
Oligonucleotides		
Mouse primers for qPCR, see Table S2	Sigma	N/A
Human primers for qPCR, see Table S3	Sigma	N/A
Deposited data		
Nanostring targeted gene expression data	This study	https://doi.org/10.6084/m9.figshare.19337429
RNA sequencing count data	This study	https://doi.org/10.6084/m9.figshare.19425302
Software and algorithms		
Quant StudioTM Real-Time PCR Software v1.3	Applied Biosystems	https://www.thermofisher.com/de/de/home/global/forms/life-science/quantstudio-6-7-flex-software.html
FACSDIVA v8.0	BD	https://www.bdbiosciences.com/en-eu/products/software/instrument-software/bd-facsdiva-software
Flowjo v10	BD	https://www.flowjo.com/solutions/flowjo
Proteome Discoverer v1.3	ThermoFisher	https://www.thermofisher.com/de/de/home/industrial/mass-spectrometry/liquid-chromatography-mass-spectrometry-lc-ms/lc-ms-software/multi-omics-data-analysis/proteome-discoverer-software.html
Sequest search engine	ThermoFisher	https://proteomicsresource.washington.edu/protocols06/sequest.php
nSolver Analysis Software	Nanostring	https://nanostring.com/products/analysis-solutions/ncounter-analysis-solutions/nsolver-data-analysis-support/
cluster v2.1.0	Maechler et al., 2019	N/A
NbClust v3.0	Charrad et al., 2014	N/A
ComplexHeatmap v.2.0.0	Gu, Eils and Schlesner, 2016	N/A
DESeq2	Love, Huber and Anders, 2014	N/A
ClusterProfiler	Yu et al., 2012	
FactoMinR	Lê et al., 2008	N/A
GraphPad Prism v8	GraphPad Software	https://www.graphpad.com/scientific-software/prism/
Others		
Analysis code RNA-seq	This study	https://doi.org/10.6084/m9.figshare.19437236
Immunopeptidomics sequences, see Table S1	This study	N/A

RESOURCE AVAILABILITY

Lead contact

Further information and requests for resources and reagents should be directed to and will be fulfilled by the lead contact, Simon Haas (simon.haas@bih-charite.de).

Materials availability

This study did not generate new unique reagents.

Data and code availability

RNA-seq count and NanoString data have been deposited at Figshare and and are publicly available as of the date of publication. DOIs are listed in the key resources table.

All original code has been deposited at Figshare and is publicly available as of the date of publication. DOIs are listed in the key resources table.

Any additional information required to reanalyze the data reported in this work is available from the lead contact upon request.

EXPERIMENTAL MODEL AND SUBJECT DETAILS

Mice

All animal experiments were approved by the Animal Care and Use Committees of the German Regierungspräsidium Karlsruhe für Tierschutz und Arzneimittelüberwachung (Karlsruhe, Germany), the Harvard Medical Area Standing Committee on Animals, the Brigham and Women's Hospital Institutional Animal Care and Use Committee (Boston, USA) or the Institutional Animal Care and Use Committees (IACUC) of the Dana-Farber Cancer Institute (Boston, USA). All mice were maintained in individually ventilated cages under SPF conditions in the animal facility of the DKFZ (Heidelberg, Germany), the Hale Building for Transformative Medicine of the Brigham and Women's Hospital (Boston, USA) or Dana-Farber Cancer Institute (Boston, USA). Wild type mice (BALB/c, C57BL/6J (CD45.2) and B6.SJL-Ptprca Pepcb/BoyJ (CD45.1)) were purchased from Harlan Laboratories, Taconic or the Jackson Laboratories. NOD.Cg-PrkdcscidIL2rgtmWjl/SzJ (NSG), C57BL/6-Tg(CAG-OVA)916Jen/J (CAG-OVA), C57BL/6-Tg(Tcra2D2,Tcrb2D2)1Kuch/J (2D2) and B6.Cg-Tg(TcraTcrb)425Cbn/J (OT-II) mice were purchased from the Jackson Laboratories. B6.129S(Cg)-Stat1tm1Dlv/J (Stat1$^{-/-}$) and B6.129S2-Il10rbtm1Agt/J (Il10rb$^{-/-}$) have been described before (Durbin et al., 1996; Spencer et al., 1998). B6.129S2-Il10rbtm1Agt/J mice were kindly provided by Dr. Laura Llaó-Cid. C57BL/6-FLT3wt/ITD/Mx1-Cre mice were kindly provided by the group of Prof. Dr. Carsten Müller Tidow. C57BL/6-Tg(TcraTcrb)1100Mjb/J (OT-I) mice were kindly provided by Stephanie Lindner from the group of Prof. Dr. Rienk Offringa. BALB/cxC57BL/6J F1 and B6-Tg(Tal1-cre)42-056Jrg H2-Ab1tm1Koni Gt(ROSA)26Sortm1(EYFP)Cos/Atp (SclCreERT2 x MHC-II-flox x Rosa26-EYFP-flox) mice were generated in house.

To induce inflammatory conditions, mice were injected intraperitoneally with a single dose of 5 mg/kg pI:C (Invivogen), 0.25 mg/kg LPS (ThermoFisher), 500U/g IFNα (Miltenyi) and MCMV (Hirche et al., 2017). For administration of ovalbumin, a single dose of 500mg/kg of full ovalbumin protein (Invivogen), 500mg/kg of DQ-OVA (Invitrogen), or 12.5mg/kg of ovalbumin 323-339 peptide (Invivogen) was administered. For knock-out induction, 100mg/kg of tamoxifen were resuspended in sunflower oil with ethanol (10%) and injected intraperitoneally once a day for five consecutive days.

Human samples

Peripheral blood and bone marrow samples from healthy donors were obtained from the University Hospital Mannheim and Heidelberg University Hospital after informed written consent using ethic application number S480/2011. Mononuclear cells were isolated by density gradient centrifugation and stored in liquid nitrogen until further use. All experiments involving human samples were conducted in compliance with the Declaration of Helsinki and approved by and in accordance with regulations and guidelines by the ethics committee of the medical faculty of the University of Heidelberg.

METHOD DETAILS

Preparation of mouse bone marrow, spleen and lymph nodes

Mouse bone marrow was prepared by crushing femur, tibia, humerus, ilium, sternum and columna vertebralis in PBS (Sigma) supplemented with 2% heat-inactivated FCS (Gibco). Subsequently, cells were filtered through 40μm cell strainers (Falcon) and erythrocyte lysis was performed for 5 min using ACK buffer (Lonza), followed by washing and centrifugation for 5 min at 250 x g. For isolation of HSPCs, cells were incubated in PBS 2% FCS for 15 minutes with antibodies against the lineage markers CD11b (M1/70), Gr-1 (RB6.8C5), CD4 (GK1.5), CD8a (53.6.7), Ter119 (Ter119) and B220 (RA3-6B2) at 4°C. Subsequently, cells were washed and incubated for 15 minutes with pre-washed anti-rat IgG-coated Dynabeads 4,5μm magnetic polystyrene beads (Invitrogen) in the ratio of 1mL of beads /mouse. Cells expressing lineage markers were depleted using a separation magnet (Invitrogen), followed by staining the remaining lineage-negative cells described below.

Spleen and lymph nodes (inguinal, axial, submandibular, mesenteric) were dissected and homogenized through a 40μm filter into PBS 2% FCS using the plunger of a syringe. Erythrocyte lysis was performed for 5 min using ACK buffer (Lonza). For CD4$^+$ T cell sorts,

the Dynabeads Untouched Mouse CD4 Cells Kit (Invitrogen) was used according to the manufacturer's instructions. Enriched cells were stained and isolated by FACS sorting as described below.

Flow cytometry staining, acquisition and FACS sorting

For flow cytometric analyses and FACS sorts, lineage-depleted, $CD4^+$ T cell enriched or unfractionated cells were stained in PBS 2% FCS for 20 min with corresponding antibodies and washed. For Y-Ae antibody conjugated with biotin, cells were washed and incubated for another 20 minutes with Streptavidin-PE (ThermoFisher). For intracellular cytokine staining, cells were stimulated for 4h at 37°C with the Cell Stimulation Cocktail (plus protein transport inhibitors) (eBioscience). After surface staining, cells were fixed, permeabilized and stained using the BD Fixation/Permeabilization Solution Kit (BD Biosciences) according to manufacturer's instructions. Finally, cells were filtered through a 35-40μM filter and acquired by a flow cytometer (LSR II or LSRFortessa, Becton Dickinson) or cell sorter (FACSAria II or FACSAria Fusion, Becton Dickinson) for analysis or sort, respectively. Common gating strategies used in this study to define populations are depicted in Figures S6 and S7.

Quantitative Polymerase Chain Reaction (qPCR)

For qPCR analyses, cells were directly sorted into RNA lysis buffer (Arcturus PicoPure RNA Isolation Kit (Invitrogen)), incubated for 30 min at 42°C and processed for cDNA synthesis using SuperScript VILO cDNA synthesis kit (Invitrogen) according to manufacturer's instructions. The newly synthesized cDNA was diluted 1:10 in RNase free H_2O and 6 μL were mixed in technical triplicates in 384-well plates with 0.5 μl of forward and reverse primer (10 μM) (Tables S2 and S3) and 7 μl PowerUP SybrGreen Mastermix (ThermoFisher). Program: 50°C for 2 minutes, 95°C for 10 minutes and 40 cycles of 95°C for 15 seconds, 60°C 1 minute. Primers were designed to be intron spanning whenever possible using the Universal ProbeLibrary Assay Design Center (Roche) and purchased from Sigma Aldrich. Experiments were performed on the ViiA7 System (ThermoFisher) and analysis of gene amplification curves was performed using the Quant StudioTM Real-Time PCR Software v1.3 (Applied Biosystems). RNA expression was normalized to the housekeepers *Gapdh*/*Actb* for murine and *B2M*/*ACTB* for human gene expression analysis. Relative expression levels are depicted in $2^{-\Delta Ct}$ values, ΔCt = (geoMean Housekeeper Ct) - (gene of interest Ct).

Murine *ex vivo* cultures

Cells were cultured at 37°C and 5% CO_2 in U-bottom plates in a total volume of 200μL of Dulbecco's Modified Eagle's Medium GlutaMAX (DMEM GlutaMAX, Gibco) supplemented with 10% heat-inactivated Fetal Calf Serum (FCS, Gibco), sodium pyruvate (1.5mM, Gibco), L-glutamine (2mM, Gibco), L-arginine (1x, Sigma), L-asparagine (1x, Sigma), penicillin/streptomycin (100 U/mL, Sigma), folic acid (14μM, Sigma), MEM non-essential amino acids (1x, ThermoFisher), MEM vitamin solution (1x, ThermoFisher) and β-mercaptoethanol (57.2μM, Sigma). Cells were sorted and, when mentioned, labelled with cell trace violet (ThermoFisher) according to manufacturer's instructions. $5x10^4$ naïve $CD4^+$ T cells were cultured with $2x10^4$ HSPCs, DCs or $CD8^+$ T cells, unless stated otherwise. When stated, ovalbumin peptides (323-339 or 257-264) (both 25μg/mL, Invivogen), full ovalbumin protein (10 mg/mL, Invivogen), DQ-OVA (100μg/mL, Invitrogen), MOG peptide (50μg/mL, Genemed Sythesis), Eα peptide (52-68) (100μg/mL, Mimotopes), LPS (100 ng/mL, ThermoFisher), αMHC-II blocking antibody (10μg/mL, M5/114.15.2, BioXCell) or a control IgG2b antibody (10μg/mL, eB149/10H5, ThermoFisher) were added to the cultures. For transwell experiments, cells were plated as described with additional $2x10^4$ HSPCs plated on 96-well plate inserts with polyester membrane and 1 μm pore size (Corning). For resting of T cells, culture medium was replaced by fresh culture medium in the absence of ovalbumin peptide, followed by culturing for two days. Re-stimulation was performed by addition of Dynabeads Mouse T-Activator (ThermoFisher) according to manufacturer's instructions.

Human *ex vivo* cultures

Human cells were cultured under the same conditions as murine cells. For T cell activation assays, $5x10^4$ naïve $CD4^+$ T cells were cultured with $5x10^3$ antigen presenting cells (either HLA-DR^+ $CD11c^+$ DCs, $CD34^+$ HSPCs or additional $CD3^+$ T cells) from an unrelated donor in the presence or absence of CytoStim (Miltenyi) or an MHC-II-restricted peptide pool (JPT) according to manufacturer's instructions. All analyses were performed after three days of co-culture using flow cytometry. For AML cell line experiments, 23 AML cell lines were characterized as stem-like (CD34, CD117, HLA-DR expression) or mature-like (CD14, CD15, CD16, CD64 expression) and co-cultured with human PBMC naive $CD4^+$ T cells in the presence or absence of CytoStim (CS) for 72h.

BM transplantation

For mouse stem cell transplantation experiments, HSPCs were transplanted intravenously into lethally irradiated (2x500rad) recipient mice together with $1x10^5$ rescue bone marrow cells. For testing of stem cell potential of MHC-II^+ populations, lineage-negative, MHC-II^+ or MHC-II^- BM cells were transplanted as described above. Four months post transplantation, total BM cells were transplanted into secondary recipients.

Mice were bled periodically and cells were stained as described above to assess engraftment. After 4 months, mice were sacrificed, analyzed for engraftment and $1x10^6$ bone marrow cells were intravenously transplanted into secondary lethally irradiated recipients. For xenotransplantation assays, HLA-DR^+ and HLA-DR^- cells from three healthy donor bone marrow aspirates were sorted, and $1x10^5$ cells were transplanted intrafemorally into sublethal irradiated (175x1rad) NSG mice. Engraftment of human cells was measured 4 months later by flow cytometry.

Adoptive co-transfer of OVA-loaded HSCs and antigen-specific T cells

$1.5x10^5$ BM OT-II $CD4^+$ T cells were sorted and intravenously transferred into Ly5.1 mice. LSK cells were isolated as described above and cultured for 12 hours in presence or absence of ovalbumin peptide (50μg/mL) in culture medium supplemented with TPO (50 ng/mL, PreproTech) and SCF (50 ng/mL, PreproTech) at 37°C, 5% CO_2 levels. Subsequently, cells were washed and ($1x10^5$ cells per mouse) adoptively transferred into the recipient mice from above. After three days, mice were sacrificed and the BM was isolated for flow cytometric analysis of HSPC-derived cells.

In vivo antigen presentation assays

For analysis of presentation of exogenous antigens on HSPCs, ovalbumin or LPS were administered to mice as described above and 1h later $4x10^4$ $CD8^+$ T cells, DCs or LSKs were isolated from mice and co-cultured with naïve OT-II $CD4^+$ T cells in the absence of exogenous ovalbumin peptide. For analysis of presentation of endogenous antigens, $CD8^+$ T cells, DCs or LSKs populations were isolated from CAG-OVA and control mice. Antigen presentation capacity was read out by co-culture with OT-II $CD4^+$ T cells in the absence of exogenous ovalbumin peptide. In a transplantation setup, WT or CAG-OVA HSPCs were co-transplanted in equal ratios into irradiated WT recipients with or without OT-II T cells at day 0 or day 60 post BM reconstitution. 20 weeks post transplantation, the BM was analyzed and total BM was re-transplanted into secondary recipients. In another setup, HSPCs were cultured for 12h with our without ovalbumin peptide and then adoptively co-transferred with freshly isolated naïve OT-II $CD4^+$ T cells, and HSPC derived progeny was analyzed after three days by flow cytometry.

MLL-AF9 experiments

LSK or GMP cells were sorted and transduced with an MLL-AF9 construct and transplanted into C57BL/6J mice (Taconic) as previously described (Krivtsov et al., 2006, 2013). In brief, LSK and GMPs were isolated from BM of C57BL/6J (wt) or C57BL/6-Tg(CAG-OVA)916Jen/J (CAG-OVA) mice cultured with retroviral supernatant for 48h. GFP^+ cells were isolated via FACS and transplanted in sublethally irradiated wt recipient mice. One month post-transplant, mice were sacrificed and leukemic GFP^+ cells were sorted and co-cultured with naïve OT-II T cells as described above and T cell activation was analyzed via flow cytometry after 72h. When indicated, $1x10^6$ naïve OT-II T cells were co-transplanted at d0 or transplanted at d15 after initial transplantation of transduced LSKs/GMPs and the disease growth in blood was measured weekly. Bone marrow and spleen of recipient mice were analyzed at the endpoint via flow cytometry.

Immunopeptidomics

Isolation of MHC ligands

$2.5x10^7$-$5x10^7$ splenocytes ($CD3^-$), T cells ($CD3^+$) or HSPCs (Lineage-$cKit^+$) were sorted and snap frozen. The MHC class II molecules were isolated using standard immunoaffinity purification (Falk et al., 1991; Kowalewski and Stevanović, 2013). In brief, snap-frozen primary samples were lysed in 10 mM CHAPS/PBS (AppliChem) with 1× protease inhibitor (Roche). For the immunoprecipitation of MHC class II–peptide complexes the monoclonal antibody M5/114.15.2 (eBioscience) covalently linked to CNBr-activated Sepharose were used (GE Healthcare). MHC–peptide complexes were eluted by repeated addition of 0.2% TFA (trifluoroacetic acid, Merck). Eluted MHC ligands were purified by ultrafiltration using centrifugal filter units (Amicon). Peptides were desalted using ZipTip C18 pipette tips (Millipore), eluted in 35 μl 80% acetonitrile (Merck)/0.2% TFA, vacuum-centrifuged and resuspended in 25 μl of 1% acetonitrile/0.05% TFA and samples stored at − 20 °C until LC–MS/MS analysis.

Analysis of MHC ligands by LC–MS/MS

Isolated peptides were separated by reversed-phase liquid chromatography (nano-UHPLC, UltiMate 3000 RSLCnano; ThermoFisher) and analyzed in an online-coupled Orbitrap Fusion Lumos mass spectrometer (ThermoFisher). Samples were analyzed in three technical replicates and sample shares of 33% trapped on a 75 μm × 2 cm trapping column (Acclaim PepMap RSLC; Thermo Fisher) at 4 μl/min for 5.75 min. Peptide separation was performed at 50 °C and a flow rate of 175 nl/min on a 50 μm × 25 cm separation column (Acclaim PepMap RSLC; Thermo Fisher) applying a gradient ranging from 2.4 to 32.0% of acetonitrile over the course of 90 min. Samples were analyzed on the Orbitrap Fusion Lumos implementing a top-speed CID method with survey scans at 120k resolution and fragment detection in the Orbitrap (OTMS2) at 60 k resolution. A mass range of 300–1500 *m/z* was analyzed with charge states $\geq$ 2 selected for fragmentation.

Database search and spectral annotation

LC-MS/MS results were processed using Proteome Discoverer (v.1.3; ThermoFisher) to perform database search using the Sequest search engine (ThermoFisher) and the murine proteome as reference database annotated by the UniProtKB/Swiss-Prot (http://www.uniprot.org), status February 2014 containing 20,270 ORFs. The search combined data of three technical replicates, was not restricted by enzymatic specificity and oxidation of methionine residues was allowed as dynamic modification. Precursor mass tolerance was set to 5 ppm, and fragment mass tolerance to 0.02 Da. False discovery rate was estimated using the Percolator node (Käll et al., 2007) and was limited to 5%. Peptide length was limited to 12–25 AA of length.

NanoString and RNA-Seq gene expression analysis

After 3 days of co-culture with $2.5x10^3$ (NanoString) or $2x10^4$ (RNA-Seq) HSPCs or $2x10^4$ DCs, $CD4^+$ T cells were FACS-sorted and lysed in RLT Buffer (Qiagen) with 1% β-mercaptoethanol (Sigma). For NanoString, RNA was hybridized with the PanCancer Mouse Immune Profiling CodeSet provided by NanoString Technologies. The barcodes were counted on an nCounter Digital Analyzer. The

obtained raw data was analyzed using the nSolver Analysis Software. For RNA-Seq, 5x10^3 T_{HSC} or T_{DC} were sorted and RNA was extracted using Arcturus PicoPure Kit, and reverse transcribed, amplified and tagmented using the SmartSeq2 protocol (Picelli et al., 2013, 2014) and using a homemade Tn5 enzyme and sequenced on an Illumina NextSeq 550 (75bp high-output). Reads were aligned to the murine reference genome (Ensembl GRCm38) using STAR v2.5.2b. Gene count tables were generated using Gencode M12 annotations. Differential expression between samples was tested using the R/Bioconductor package DESeq2 (Love, Huber and Anders, 2014). GSEA was run with the R/Bioconductor package clusterProfiler (Yu et al., 2012) and PCA was performed with FactoMineR (Lê et al., 2008).

In vitro suppression assay

T_{DCs} and T_{HSCs} were generated by 3 days of culture as described above, rested in the absence of ovalbumin peptide for 2 days and FACS-sorted. Subsequently, 10^5 CTV-labelled naïve bystander CD4$^+$ or CD8$^+$ T cells were cultured with 10^5 CD19$^-$CD3$^-$ splenocytes and different ratios of *in vitro*-generated T_{HSCs} or T_{DCs}, or freshly purified CD4$^+$ T_{regs} relative to the amount of naïve bystander CD4$^+$ T cells, and soluble anti-CD3 antibody (1 μg/mL,145-2C11, BioXCell). Cells were analyzed by flow cytometry and proliferation of bystander cells was assessed.

$$Suppression\ Index = \frac{\text{Sample Cell Trace Violet gMFI}}{\text{No T cell activation control Cell Trace Violet gMFI}}$$

$$Proliferation\ Index = \frac{\Sigma\left(\frac{number\ of\ cells\ in\ i}{2^i}\right)}{\Sigma\left(\left(\frac{number\ of\ cells\ in\ i}{2^i}\right) - (number\ of\ cells\ in\ i = 0)\right)}$$

i = Number of cell divisions, seen by CTV dilution

In vitro CD8$^+$ T cell cytotoxicity assay

5x10^4 CTV-labelled naïve OT-I CD8$^+$ T cells were co-cultured with 5x10^4 naïve OT-II CD4$^+$ T cells and 2x10^4 CD19$^-$CD3$^-$ splenocytes or HSPCs in the presence or absence of the MHC-I- and/or MHC-II-restricted OVA peptides. T cells and APCs were analyzed after 3 days via flow cytometry. Cytotoxicity was measured by annexin V positivity in the APCs.

In vitro macrophage polarization assay

T_{DCs} and T_{HSCs} were generated by 3 days of culture as described above, rested in the absence of ovalbumin peptide for 2 days and FACS-sorted. Subsequently, 5x10^4 freshly sorted T_{DCs} or T_{HSCs} were cultured with 1x10^5 CD19$^-$CD3$^-$CD11b$^+$SSC^{low} bone marrow monocytes and macrophages and anti-CD3/anti-CD28 activating beads according to manufacturer's instructions. Cells were analyzed after 24 hours by flow cytometry.

In vivo suppression assay

For the *in vivo* suppression assay, T_{DCs} and T_{HSCs} were generated as described above and FACS sorted at day 3 of the co-culture. Subsequently, 1.5x10^5 cells were adoptively transferred intravenously together with 10^6 CTV-labelled naïve OT-II CD4$^+$ T cells into naive mice. One day post transfer, mice were injected with ovalbumin peptide and LPS as described above, and splenic T cells were analyzed after 3 days via flow cytometry. The proliferation index was calculated as described above.

EuroFlow analysis of diagnostic AML samples

Diagnostic bone marrow aspirates of AML patients were analyzed using the EuroFlow panels (van Dongen et al., 2012) at the University Hospital Heidelberg, Germany. AML blast cells were gated in FlowJo as CD45$^+$ excluding CD45^{high}SSC^{low} healthy lymphoid cells, and geometric mean fluorescence intensities (gMFIs) for all FACS markers were exported. Before z-score scaling the data, values larger than the 95 percentile and smaller than the 5th percentile were considered to be outliers and adjusted to the 95th or 5th percentile, respectively. The data was partitioned into 4 clusters by PAM (partitioning around medoids) clustering using the R package cluster v2.1.0 (Maechler et al., 2019), after determining the best number of clusters using NbClust v3.0 (Charrad et al., 2014). Heatmap visualizations of the data were done using the R/Bioconductor package ComplexHeatmap v.2.0.0 (Gu, Eils and Schlesner, 2016). Stem-, Mono-, and Granulo-indices were calculated by adding the scaled gMFIs of the respective signature for each patient and min-max feature scaling each index between patients: Stem-index = CD34 and CD117, Mono-index = CD14, CD64, CD300e and CD45, Granulo-index = CD35, CD15, CD16 and SSC-A.

Quantification and statistical analysis

Flow cytometric analyses were performed in FlowJo (BD). Bioinformatic analyses were performed in R, and visualized or further analyzed in R or GraphPad Prism (v8.4.2, GraphPad Software). The vast majority of ex vivo experiments have been performed multiple times. Most experiments for large-scale gene and protein expression analyses and in vivo experiments, have been performed once. The number of biological replicates per experiment are indicated in the figure legends. Statistical tests used in every figure

legend. In short, one- or two-way ANOVA, or Kruskal-Wallis tests were performed as discovery tests wherever necessary. Only when the discovery test was significant, post-hoc two-tailed t-tests or Mann-Whitney tests were performed based on normality of the data. In case of multiple comparisons, p-values were corrected by the Benjamini-Hochberg false discovery rate of 5% and q-values were subsequently used to indicate significance. Significance is depicted as: no significance = ns, $P<0.05$ *, $P<0.01$ **, $P<0.001$ ***, $P<0.0001$ **** according to statistical tests indicated in each figure legend.